Answers to Anonymous Referee 1

In order to make answers as clear as possible, we copy in black the reviewer comments, and answer with blue color. Proposed changes in the original text are indicated in red.

Anonymous Referee #1
Received and published: 20 March 2019

Review of Lamarque and Julia, Solid Earth Discussions, 2019

This paper calculates teleseismic P-wave receiver functions to investigate the depth dependence of seismic anisotropy in the crust and lithospheric mantle in NE Brazil. The analysis considers the back-azimuth variations in observed receiver function signal and performs a harmonic decomposition to provide a quantitative estimate of anisotropy in terms of: 1) a plunging axis of symmetry and/or dipping interface; or 2) a horizontal axis of symmetry. The depth decomposition of the anisotropy is able to retrieve the average anisotropy in the crust and lithospheric mantle. The results show consistent anisotropy in the crust and mantle, indicating a control by lithospheric-scale shear zones that develop during the Brasiliano-Pan African orogeny. The lack of well characterized anisotropy at some stations is taken as an indication of re-heating of the lithosphere by an asthenospheric channel. Stations along the Atlantic coast resolve fast anisotropic directions perpendicular to the margin, suggesting lithospheric inheritance during rifting.

General comments:

The paper compiles all available receiver function (RF) data and calculates new RF data for 11 recently installed stations. The RF analysis is adequately described and follows the standard procedures to obtain high-quality data. The novelty of this paper lies in the application of the harmonic decomposition to reveal depth-dependent anisotropy from back-azimuthal variations in the amplitude of both radial and tangential components of RF data, for individual stations. The results are discussed in an appropriate way, although part of the methodology lacks reference to original work that implemented variants of the technique (see specific comments). The condition for rejecting anisotropy (and therefore interpreting the subsurface structure as isotropic) could also be subject to debate. Overall the paper addresses an important question about the structure of fabrics beneath NE Brazil in relation with lithospheric inheritance and the significance of lithospheric-scale shear zones.

We greatly thank the reviewer for a detailed reading of our manuscript. In particular, we appreciate the remark on our interpretation of the stations with large variability in anisotropic parameters, which helped us improve our interpretation of the results and their geodynamic implications.

Specific comments:

The discussion of RF analysis is appropriate and includes proper referencing up to line 19 on page 7. There the authors describe an additional preliminary step in the harmonic decomposition analysis, where they migrate the time signals to

depth using a 1D seismic velocity model to correct for the move-out of teleseismic waves. The migration to depth (before harmonic decomposition) was first proposed by Bianchi etal. (2010), who performed common-conversion (CCP) stacking using a dense line of stations and carried out the decomposition at CCP points. This method was further applied in Piana Agostinetti et al. (2011) and Piana Agostinetti and Miller (2015). The step proposed here by the authors (converting time to depth at individual stations, as opposed to CCP stacking), was proposed by Audet (2015) and further applied in Cossette et al. (2016) and Tarayoun et al. (2017). The optimization of energy on one of the k=1 components (as done here) was also proposed by Audet (2015) to retrieve the dominant angle of anisotropy.

The reviewer is correct when pointing out that migration before harmonic stripping was already proposed in previous works. We have added the missing references to the updated manuscript. The proposed change in the text is:

« Prior to implementing the anisotropy analysis, each radial and tangential receiver function was migrated to depth after P to S ray-tracing through the global velocity model ak135-f (Kennett et al., 1995; Montagner and Kennett, 1996). The purpose of the migration is to correct the phase move-out introduced by varying incidence angles among the incoming teleseismic P-wavefronts, effectively equalizing the receiver function waveforms in the depth domain (Dueker and Sheehan, 1997). Migration before harmonic stripping at individual stations was previously utilized by Audet (2015), Causette et al. (2016) and Tarayoun et al. (2017). Similarly, Bianchi et al (2010), Piana Agostinetti et al (2011), and Piana Agostinetti and Miller (2015) applied harmonic decomposition on depth-migrated cross-sections obtained through CCP stacking of receiver functions. Next, the migrated radial and transverse receiver functions for each station were grouped by back-azimuth in 36 non-overlapping, ...»

On page 10, the authors discuss the reliability of the anisotropic directions using a bootstrap analysis and consider that a measurement is unreliable if the bootstrap uncertainty is greater than 20 degrees. The bootstrap analysis returns an estimate of the standard error on the mean value on modeled parameters (such as the dominant angle of anisotropy), and confidence intervals are normally calculated from the standard error. Is this what is meant by “uncertainty” here? Is it 1-sigma (68% confidence) or 2-sigma (95%)?

Uncertainties refer to the 2-sigma standard error obtained from a population of 200 angle estimates developed from bootstrapping the original dataset. Additional text will be added to the manuscript to clarify that point:

« In order to estimate uncertainties, we applied a bootstrap statistical approach by randomly re-sampling with replacement our receiver functions. We performed such analysis with 200 replications at each of the selected stations. From these 200 values, we estimated the standard error (2-sigma), which corresponds to the uncertainty in the direction of the fast-axis of symmetry. A measurement is considered as not reliable, and then rejected, if the estimated uncertainties are larger than 20°.

Furthermore, large variability in the recovered angle might not necessarily imply that the medium is isotropic. Strong structural heterogeneity might

produce large-amplitude signal with apparent back-azimuth distribution with k>2. Alternatively, crystal symmetries might not always produce seismic anisotropy that can be modeled with the k=1 or k=2 components. So, it is still of interest to show the strength of the signal on the k=1 and k=2 energy components despite the large variability in bootstrap angles. Following up from this comment, Figure 6 could be improved by plotting the relative amplitude of the corresponding energy components. On the maps, the anisotropy (length of bars) appears to be equal in magnitude at all stations, though I suspect that the energy components vary significantly from one station to another and regionally. This additional piece of information could also be included in the Discussion and compared with SKS splitting results. Finally, it would be insightful to look at the receiver functions before application of the harmonic decomposition (e.g., in back-azimuth panels) to see why the "unreliable" stations have large uncertainty in anisotropic direction. This could be added to the Supplementary Information.

The reviewer is correct that large variability in the recovered angles at «unreliable» stations is not necessarily related to weak anisotropy under those stations. Following her/his advice, we have now calculated the energy and inspected transverse component amplitudes in detail. We found that energy at the "unreliable" stations is as strong as that found at the "reliable" ones (see results for station cs6b in the additional supplementary material). To make this clear, Figure 6 has been updated to display energy level at each station (for clarity reasons, we prefer to keep constant bar lengths and denote energy through color-coding the station symbol). The new legend for Figure 6 will be:

« A) Map of symmetry directions (dark lines) obtained for the crust (0-32 km). When one line is plotted at the station, it represents either the trend of the dip, in the case of dipping interface, or the trend of the fast axis in the case of plunging anisotropy. When two lines are plotted, they refer to the fast axis and to its perpendicular direction for horizontal anisotropy. Light colors represent 2σ uncertainties estimated from the bootstrap (after re-sampling 200 times). B) Same as for the lithospheric mantle (32-100 km). Station symbols have been color-coded according to the energy level of the dominant harmonic degree. »

It is now clear that our original interpretation of large angle variability as resulting from a weak anisotropic signature under the station was incorrect. We agree with the reviewer that non-azimuthal anisotropy and/or strong structural heterogeneities provide a more likely explanation. In any case, this non-azimuthal anisotropy is still located above a NE-SW trending channel of thin lithosphere and shallow asthenosphere. Accordingly, we now propose that deformation from thermo-mechanical erosion by horizontal, sub-lithospheric flow - previously postulated in the tomographic study of Simões Neto et al. (2019) - must be ongoing above the NE-SW channel. Also, as initial thinning of the lithosphere along the channel was probably triggered by Mesozoic extension along the Cariri-Potiguar trend, alterations of the original Precambrian anisotropic fabric by Mesozoic extension might still be present above the channel. Additionally, we note that the location of the Cariri-Potiguar trend also marks the boundary between the EW striking shear zones in the southern Province from the NE-SW striking shear zones in the western Province (Figure 1). This suggests the Cariri-Potiguar trend also marks the location of a

former paleo-suture that later acted as a zone of weakness along which the Mesozoic rift (now aborted) developed.

Thus, we believe the non-azimuthal anisotropy recorded at stations located along this trend is more likely related to complex fossil anisotropic fabrics resulting from a combination of deformation along the ancient collision between Precambrian blocks, Mesozoic extension, and thermo-mechanical erosion/mantle dragging by sub-lithospheric flow.

Modifications within the manuscript :
« ~~5.3 Asthenospheric flow heating the lithosphere~~
5.3. Non-azimuthal anisotropy along the aborted Cariri-Potiguar rift
At a number of stations (ar05, nbma, pfbr, nbpa, cs6b), uncertainties for the direction of the fast axis of anisotropy are larger than 20°. ~~We think that anisotropy is just too small to be confidently retrieved, and interpret those stations as sampling an isotropic lithosphere. These stations record signal on the tranverse component (see example for station cs6b in supplementary materials, Figure S3) , indicating the presence of anisotropy at depth. Energy on k=1 or k=2 is of similar intensity to the energy at stations with smaller uncertainties, as displayed in Figure 6.~~ Interestingly, those stations seem to form a remarkable line trending NE-SW that approximately coincides with the location of the Cariri-Potiguar trend. Stations nbta and pcse also seem to align along the same direction more to the East. ~~One explanation for the absence of lithospheric-scale anisotropy could be the destruction of anisotropic fabrics through sub-lithospheric heating of the overlying lithosphere. This hypothesis was proposed for the Cameroon Volcanic Line (CVL) by Deplaen et al. (2014), who argued that hotspot tectonism associated with the Mesozoic opening of the South Atlantic may have thermomechanically eroded Precambrian age fossil lithospheric fabrics beneath the CVL. Indeed, the presence of relatively shallow asthenosphere north-west of the Borborema Plateau has been recently postulated from a P-wave tomography study of the Borborema Province (Simões Neto et al., 2019). These authors identified a NE-SW trending low-velocity channel bordering the Plateau that closely coincides with the observed isotropic alignment. Moreover, independent SKS splitting measurements performed at those stations by Bastow et al. (2015) reported either null measurements (stations nbma, cs6b, nbta) or really weak anisotropy (stations pfbr and nbpa).~~ This NE-SW oriented line is located above a NE-SW trending channel of thin lithosphere imaged by the tomographic study of Simões Neto et al. (2019). We suggest that deformation from thermo-mechanical erosion by horizontal, sub-lithospheric flow along the channel - also postulated by Simões Neto et al. (2019) - must be ongoing above this NE-SW channel. Also, as initial thinning of the lithosphere along the channel was triggered by Mesozoic extension along the Cariri-Potiguar trend, alterations to the original Precambrian anisotropic fabric by Mesozoic extension might still be present. Additionally, we note that the location of the Cariri-Potiguar trend also marks the boundary between the EW striking shear zones in the southern Province from the NE-SW striking shear zones in the western Province (Figure 1). This suggests the Cariri-Potiguar trend also marks the location of a former paleo-suture that later acted as a zone of weakness along which the Mesozoic rift (now aborted) could develop. Thus, we believe the non-azimuthal anisotropy recorded at stations located along this trend is likely related to complex fossil anisotropic fabrics resulting from a combination of deformation along the ancient collision between Precambrian blocks, Mesozoic extension, and thermo-mechanical erosion/mantle dragging by sub-lithospheric flow. »

Technical corrections:

Page 8, line 3: “presents” -> present.
Done.

Page 10, lines 6 and 10: the interval “[0,2]” ->. Do you mean [0, 2pi]?
Yes, it’s been modified accordingly.

Page 11, line 2: “Realize that” -> We note that
Done.

Page 12, line 3: “mantellic” -> mantle
Done.

Caption of Figure 6. It’s not clear to me why the direction perpendicular to the fast axis is required in the case of horizontal anisotropy. Is it to differentiate between k=1 and k=2 directions? Which one of the two is the fast axis?

In the case of anisotropy with pure horizontal fast axis of symmetry, the energy is only on the k=2 harmonics and receiver functions display a 4-lobed back-azimuthal pattern. A synthetic example of that case is visible in Schulte Pelkum and Mahan (2014), Figures 2a and 3a. This 4-lobed back-azimuthal pattern implies maximum amplitudes for 4 directions, which correspond to: (i) the direction of the fast axis of symmetry, (ii) the direction opposite to the fast-axis of symmetry, (iii) the direction perpendicular to the fast axis of symmetry, and, (iv) the direction opposite to the perpendicular. It is thus not possible to discriminate between the fast axis of symmetry and the direction perpendicular to it through analysis of the k=2 harmonics.

Page 14, line 14: “Bastow et al. (2011); Assumpçao et al. (2011)” -> Bastow et al.(2011) and Assumpçao et al. (2011)
Done.

Page 14, line 22: “sensible” -> sensitive
Done.

References (not appearing in paper):
Cossette et al.: Structure and anisotropy of the crust in the Cyclades, Greece, using receiver functions constrained by in situ rock textural data, J. Geophys. Res., 121,2661-2678 (2016).
Piana Agostinetti et al.: Fluid migration in continental subduction: The Northern Apen-nines case study, Earth Planet. Sci. Lett., 302-267-278 (2011).
Piana Agostinetti and Miller: The fate of the downgoing oceanic plate: Insight from the Northern Cascadia subduction zone, Earth Planet. Sci. Lett., 408, 237-251 (2015).
Tarayoun et al.: Architecture of the crust and uppermost mantle in the northern Canadian Cordillera from receiver functions, J. Geophys. Res., 122, 5268-5287 (2017).

All the missing references have now been added to the reference list.

Answers to Anonymous Referee 2

In order to make answers as clear as possible, we copy in black the reviewer comments, and answer with blue color. Proposed changes in the original text are indicated in red.

Anonymous Referee #2
Received and published: 5 April 2019

The manuscript under review presents a detailed accounting of lithospheric anisotropy through the use of Ps receiver function analysis and data collected at 75 seismic stations within the Borborema Province of NE Brazil. The importance of their analysis rests in the fact that they can provide firm constraints on anisotropic boundary depth, in contrast to shear wave splitting which is a path integrated measurement. Their results show a clear correlation between tectonic deformation and orientation of seismic anisotropy. Within the continent, they find that the orientation of anisotropy is coincident with the orientation of large-scale shear zones thought to be associated with the Brasiliano-Pan African Orogeny. On the coast, anisotropy is oriented perpendicular to the coastline, suggesting that rifting is the process responsible for generating anisotropy. In places where anisotropy is absence, it is inferred that heating by the asthenosphere may have destroyed any preexisting lithospheric fabric.

Comments regarding methodology: Overall, the methodology is thoroughly and carefully described, and proper citations were given. My only question is regarding the cut-off for the minimum number of bins with data (lines 24-26). The authors require a minimum of 9 bins with data (90 degrees), which can be either continuous or discontinuous. Why was this minimum chosen? Is there an appreciable difference in how well the harmonic decomposition works? Do the authors have synthetic example they could show to demonstrate their reasoning? The reason I ask is because this seems to be the primary reason for reducing the number of stations from 75 to 39.

The reason for selecting stations that display data in at least 9 bins (10 degrees wide) is purely geometrical. Recall that we use receiver functions to map anisotropy with either 2-lobed (plunging fast axis of symmetry) or 4-lobed (horizontal fast axis of symmetry) back-azimuthal patterns. In the case of a plunging fast axis of symmetry, 9 bins corresponds to half the period for a 2-lobed pattern (90 degrees); in the case of a horizontal fast axis of symmetry, 9 bins corresponds to a full period for a 4-lobed pattern (90 degrees). By requiring 9 bin coverage (10 degree wide), we are able to reliably display either a 2-lobed or a 4-lobed pattern.

We propose to modify the text in the manuscript as:

« Next, the migrated radial and transverse receiver functions for each station were grouped by back-azimuth in 36 non-overlapping, 10° wide bins, and averaged within each bin. A given station was then selected if it presented at least two averaged receiver functions (one radial and one tangential) in at least 9 bins. This selection criterion ensured a sampling of at least 90° in back-azimuth, either continuously or discontinuously, around the station. A back-azimuthal coverage

from at least 9 bins (each 10° wide) allows the mapping of either half the period for a 2-lobed pattern (anisotropy with plunging fast axis of symmetry) or a full period for a 4-lobed pattern (anisotropy with horizontal fast axis of symmetry). A total of 39 stations were thus selected for anisotropy analysis. An example of stacked and migrated receiver functions is displayed in Figure 4. »

Comments regarding results: I appreciated the inclusion of the harmonically decomposed results within the supplementary materials. They clearly exhibit evidence of anisotropy. I did however wonder how the authors dealt with cases where more than one anisotropic boundary was present within either the crust or the mantle. I may have missed where they spoke to this, but could not find it upon reexamining the manuscript. A clearer description would have been greatly appreciated.

Our goal in this paper is to examine the direction of the dominant anisotropy within two depth windows, which correspond to the crust and the lithospheric mantle. We make the assumption that in the case of several anisotropic layers, the layer with the strongest anisotropy will dominate the results. We are aware that results can reflect the average value from different anisotropic layers, or from different types of anisotropy in the case of similar anisotropic strength.

We propose to modify the text in the manuscript as:

"4. Results
Anisotropy parameters were examined for each station at two depth-window ranges: (1) crust (Figure 6A), which was assumed to be located between 0 and 33 km depth, in agreement with the 32-40 km range estimated by Luz et al. (2015b) under the Borborema Plateau and 30-33 km under the surrounding basins; and (2) lithospheric mantle, which was taken to be between 33 and 100 km depth (Figure 6B). We assume that the layer with the strongest anisotropy will dominate the results in the case of several anisotropic layers. However, it might happen that results reflect the average value from different anisotropic layers, or from different types of anisotropy in the case of similar anisotropic strength. All results are indicated in Table 1.
An inspection of Figure 6A reveals that the crust of northeast Brazil ..."

Comments regarding interpretation: My only significant concern with the manuscript was that while regional patterns of deformation matched the fast direction, it was not always clear to me that the material properties would necessitate such an answer. For example, while the LPO of olivine typically means that the A-axis of olivine is oriented in the same direction as strain, the crust is significantly more complex, as several candidate minerals can generate different types of anisotropy, in addition to the possibility of shape preferred orientation of different materials. I would encourage the authors to think more carefully about crustal anisotropy in particular.

We agree with this remark. A complex combination of LPO and SPO could be present in the mantle, although LPO is likely to dominate (Nicolas and Christensen, 1987; Silver 1996; Mainprice et al., 2000); fractures and cracks or fine layering, could additionally contribute in the crust. For that reason, our

interpretations focus dominantly on mantle anisotropy, consistency of anisotropy within the lithosphere (crust and mantle), and regional-scale trends. And, to avoid a bias related to local features, we refrain from interpreting small-scale variations in anisotropy within the crust.

Comments regarding figures: Figure 6: It would be useful if the names of the stations were more clearly written as they appear washed out and are difficult to read.
Done.

References :
* Mainprice D., Barruol G.. Ben Ismaïl W.. Karato S.-I., Forte A., Liebermann R., Masters G., Stixrude L.. The seismic anisotropy of the Earth's mantle: from single crystal to polycrystal, Earth's Deep Interior: Mineral Physics and Tomography From the Atomic to the Global Scale, 2000 American Geophysical Union doi:10.1029/GM117p0237
* Nicolas A., Christensen N.I.. Froidevaux K., Fuchs C.. Formation of anisotropy in upper mantle peridotites: A review, Composition, Structure and Dynamics of the Lithosphere, 1987 Asthenosphere System (pg. 111-123)
* Silver P.G.. Seismic anisotropy beneath the continents: probing the depths of geology, Annu. Rev. Earth planet. Sci., 1996, vol. 24 (p. 385-432)

Lithospheric and sub-lithospheric deformation under the Borborema Province of NE Brazil from receiver function harmonic stripping

Gaelle Lamarque[1,2] and Jordi Julià[1,3]

[1]Programa do Pós-Graduação em Geodinâmica e Geofísica, Universidade Federal do Rio Grande do Norte, Natal, RN CEP 59078-090, Brazil
[2]Ifremer, Geosciences Marines, Centre de Brest, 29280 Plouzané, France
[3]Departamento de Geofísica, Universidade Federal do Rio Grande do Norte, Natal, RN CEP 59078-970, Brazil

Correspondence: Gaelle Lamarque (gaelle.lamarque@ifremer.fr)

Abstract. The depth-dependent anisotropic structure of the lithosphere under the Borborema Province of northeast Brazil has been investigated through harmonic stripping of receiver functions developed at 39 stations in the region. This method retrieves the first (k=1) and second (k=2) degree harmonics of a receiver function dataset, which characterize seismic anisotropy beneath a seismic station. Anisotropic fabrics are in turn directly related to the deformation of the lithosphere from past and current tectonic processes. Our results reveal the presence of anisotropy within the crust and the lithospheric mantle throughout the entire Province ~~, with the exception of a few stations in the continental interior that lack evidence for any anisotropic signatures~~. Most stations in the continental interior report consistent anisotropic orientations in the crust and lithospheric mantle, suggesting a dominant NE-SW pervasive deformation along lithospheric-scale shear zones developed during the Brasiliano-Pan African orogeny.~~The lack of anisotropy at a few stations along a NE-SW trend in the center on the Province is harder to explain, but might be related to heating of the lithosphere by an asthenospheric channel.~~ Several stations aligned along a NE-SW trend located above the (now aborted) Mezosoic Cariri-Potiguar rift display large uncertainties for the fast-axis direction. This non-azimuthal anisotropy may be related to a complex anisotropic fabric resulting from a combination of deformation along the ancient collision between Precambrian blocks, Mesozoic extension and thermo-mechanical erosion dragging by sub-lithospheric flow. Finally, several stations along the Atlantic coast reveal depth-dependent anisotropic orientations roughly (sub)perpendicular to the margin. These results suggest a more recent overprint, probably related to the presence of frozen anisotropy in the lithosphere due to stretching and rifting during the opening of the South Atlantic.

1 Introduction

Understanding intraplate deformation and its relationship to deep geodynamic processes such as sublithospheric flow is critical for improving our understanding of the evolution of continents. The Borborema Province of NE Brazil, for instance, has witnessed several cycles of deformation, as well as recurrent episodes of intraplate volcanism and uplift, during its geological history. Brasiliano-Pan African deformation is well represented through the network of shear zones that pervade the Borborema Province (Vauchez et al., 1995; Neves et al., 2000). These shear zones separate several tectonic terrains of Paleoproterozoic and Archean age that amalgamated and/or were reworked during the orogeny (Jardim de Sá et al., 1992; Cordani et al., 2003). Major Neoproterozoic shear zones thus constitute inherited structures that could have influenced the geometry of subsequent tectonic processes, such as the opening of the South Atlantic Ocean (Tommasi and Vauchez, 2001; Kirkpatrick et al., 2013). Also, current topography of the Borborema Plateau and the Sertaneja Depression may have resulted from a combination of on-going deep processes, such as edge-driven convection in the asthenospheric mantle and/or stretching and thinning of the lithosphere during Mesozoic times (de Oliveira and Medeiros, 2012; Almeida et al., 2015).

Recent seismological studies from receiver functions (Almeida et al., 2015; Pinheiro and Julia, 2014; Luz et al., 2015a, b), ambient noise (Dias et al., 2014) or P-wave tomography (Simões Neto et al., 2019), and SKS splitting (Bastow et al., 2015) have greatly contributed to further our understanding of the relationships between inherited Precambrian structures, Mesozoic extensional processes, and episodes of post-breakup volcanism and uplift. However, several tectonic and geodynamic questions remain unanswered. In particular, the presence of the Meso-Cenozoic Macau-Queimadas volcanism (MQA, figure 1) - which does not present a clear age progression - remains unclear. Moreover, SKS-waves showed little to no evidence of splitting in the continental interior (Bastow et al., 2015), which is difficult to comprehend given the complex tectonic and deformational history of the Province.

Here, we determine depth-dependent anisotropy in the Borborema lithosphere (crust and mantle) from harmonic analysis of receiver functions. Our results confirm that SKS splitting at coastal stations is dominated by fossil anisotropic fabrics in the lithospheric mantle, likely originating from Mezosoic extension. In the continental interior, receiver function stripping reveal fast-axis orientations consistent with major regional shear zones, suggesting their continuation at depth into the lithospheric mantle. Our results also confirm the absence of lithospheric (fossil) anisotropy under stations that did not record SKS-splitting. These stations are aligned along a NE-SW trend located west and north of the Borborema Plateau, a high-standing topographic feature that rises $\sim$1000 m above mean sea level. We argue that the absence of anisotropy in the lithosphere is related to sub-lihospheric heating of the overlying lithosphere by a shallow asthenospheric channel under the Province.

2 Geological setting

The Borborema Province formed during the Neoproterozoic Braziliano/Pan-African orogeny (600-580 Ma), as a result of the collision between the São Luiz-West Africa craton to the north and the São Francisco-Congo craton to the South (Jardim de Sá et al., 1992; Cordani et al., 2003). It thus represents the west central portion of a larger Neoproterozoic belt that resulted from the assembly of the Gondwana supercontinent.

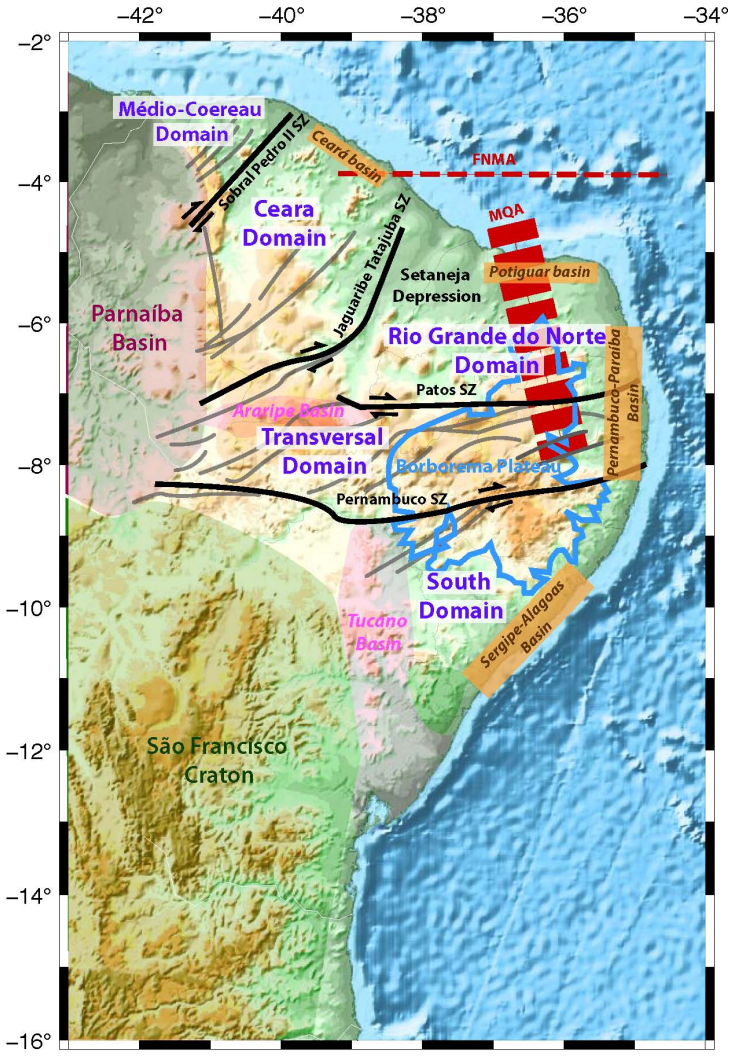

Figure 1. Topographic map of northeast Brazil with main geological features of the Borborema Province superimposed. Black and grey lines correspond to major shear zones (SZ) and red dashed lines to the volcanic alignments of Fernando de Noronha-Mecejana (FNMA) and Macau-Qeimada (MQA). The Borborema Plateau boundaries are indicated in blue.

The basement of the Borborema Province comprises mostly gneisses and migmatitic rocks of Paleoproterozoic age, and small Archean nuclei, overlain by Neoproterozoic metasediments formed during the Brasiliano orogeny (Neves, 2003). This basement is affected by an extensive network of Neoproterozoic shear zones oriented EW and NE-SW (Figure 1). These shear zones are major structures several hundreds of kilometers long and tens of kilometers wide (Vauchez and da Silva, 1992) that can be traced into the African continent in paleogeographic reconstructions (Arthaud et al., 2008). The Borborema shear zones were activated in high temperature and high-to-low pressure conditions and are associated with a strong production of

magmas from both crustal and mantle sources (Vauchez et al., 1995). The shear zone network can be split into two domains: a western domain of NE-striking skike-slip faults, and an eastern domain of more sinuous, discontinuous E-W-striking shear zones (Vauchez et al., 1995). These two domains could be related to two discrete collisional events with the Parnaíba block to the west and the São Francisco craton to the south, respectively, which forced NE extrusion of the Province at the end of the Neoproterozoic (Araújo et al., 2014).

The geodynamic evolution of this basement and the significance of these shear zones is still debated, and two main models have been traditionally proposed. On one hand, the accretionary model proposes that the Borborema Province comprises of several Paleoproterozoic small continental fragments that aggregated along the shear zones, which then constitute lithospheric-scale suture zones separating independent tectonic blocks (Cordani et al., 2003; Van Schmus et al., 2011; Araújo et al., 2014). The number of independent terrains is unclear, but there is a general consensus in arranging them into five major Precambrian domains: (i) Médio-Coereau, in the northwestern most tip of the Province; (ii) Ceará, between the Sobral-Pedro II and Jaguaribe-Tatajuba shear zones; (iii) Rio Grande do Norte, immediately east of the Ceará domain; (iv) Transversal or Central, between the Patos and Pernambuco lineaments; and (v) Southern, immediately north of the São Francisco craton (Figure 1). On the other hand, it has been suggested that the Borborema Province was a single unit since 2.0 Ga and that the shear zones recorded intracontinental supracrustal deformation during the Brasiliano orogeny (Tommasi et al., 1995; Vauchez et al., 1995; Neves, 2003). In this later model, micro-plate amalgamation largely predates the Brasiliano orogeny, which would have only partially reworked preexisting plate structures in the Borborema Province.

During the Mezosoic, opening of the south Atlantic separated the Borborema Province from its African conjugate (de Matos, 1992). Continental rifting resulted in significant crustal thinning in the region (Santos et al., 2014; Lima Neto et al., 2013; Luz et al., 2015b), forming both marginal (e.g. Ceará, Potiguar, Pernambuco-Paraíba, Sergipe-Alagoas) and intra-continental (e.g. Araripe, Tucano) sedimentary basins (Figure 1). The post Gondwana breakup evolution of the Borborema Province is characterized by recurrent magmatism (Knesel et al., 2011) and postulated episodes of uplift in the Borborema Plateau (Morais Neto et al., 2009; de Oliveira and Medeiros, 2012) and the Araripe basin (Assine, 2007; Marques et al., 2014). Intraplate volcanism is characterized as small-volume, long-lived and mainly alkalic in nature (Knesel et al., 2011). It is arranged along two main linear alignments of Mesozoic-Cenozoic volcanic rocks (Figure 1): the Macau-Queimadas Alignment (MQA), mostly on-shore and approximately trending in the north-south direction; and the Fernando de Noronha-Mecejana Alignment (FNMA), mostly off-shore and trending in the east-west direction (Mizusaki et al., 2002; Knesel et al., 2011, and references therein). The MQA displays K/Ar ages ranging from 80 to 30 Ma (Mizusaki et al., 2002) and 40Ar/39Ar ranging from 93 to 7 Ma (Knesel et al., 2011) without a clear age progression, whereas the FNMA displays progressive K/Ar and 40Ar/39Ar ages from the Fernando de Noronha archipelago (22 to 2 Ma) to the west (Knesel et al., 2011, and references therein), to the Mecejana volcanism (34 to 26 Ma) to the east (Mizusaki et al., 2002).

Cenozoic uplift along the northeastern brazilian margin was inferred from ~~both~~ relative dating of elevated sediments of the Serra dos Martins formation ~~in the northern Borborema Province and~~, absolute dating from apatite fission-track analysis of granitic-gneissic and sedimentary samples and geomorphological studies ~~(Morais Neto et al., 2009; Morais Neto et al., 2012)~~ (Morais Neto et al., 2009; de Oliveira and Medeiros, 2012; da Nóbrega et al., 2005; Nogueira et al., 2015). Although some sort

of tectonic uplift and/or inversion of the Araripe basin seems to be widely accepted (Marques et al., 2014; Peulvast and Bétard, 2015; Garcia et al., 2019), uplift in the Borborema Plateau is more debated. On one hand, de Oliveira and Medeiros (2012) argue that this tectonic event is linked to Cenozoic mafic underplating and isostatic uplift due to a small-scale convection cell at the edge of the continent, which might have also been responsible for the surface volcanism (Knesel et al., 2011). The hypothesis of a thin layer of mafic underplate seems to be consistent with recent receiver functions observations south of the Patos Lineament (Luz et al., 2015b, a). However, Luz et al. (2015b) debated the time of emplacement of such a mafic cumulates. These authors proposed that this mafic layer would be part of the original Proterozoic crust, and that the southern Borborema Plateau should be regarded as a high-standing, rheologically strong block surrounded by stretched and delaminated crust. The stretching model seems to have been confirmed by a rheological contrast along the Patos lineament postulated from seismic P-wave tomography (Simões Neto et al., 2019). The tomographic study also identifies an asthenospheric low-velocity channel trending NE-SW under the center of the Province, which is interpreted as resulting from lateral flow from a distant mantle plume. Such asthenospheric flow might represent the source of Meso-Cenozoic intraplate volcanism in NE Brazil.

3 Data and methodology

3.1 Seismic data

Seismic data for this study were obtained at 75 seismic stations in northeast Brazil. These stations belong to a variety of seismic networks, both permanent and temporary. The Rede Sismográfica do Nordeste (RSISNE) consists of 19 broadband stations equipped with RefTek 151-120 sensors feeding RT-130 digitizers (24-bit) sampling at 100 Hz, with an inter-station spacing of about 250 km and a network aperture of $\sim$800 km. The RSISNE network has been in operation since 2011 and was initially funded by the national oil company Petrobras. The Instituto Nacional de Ciência e Tecnologia em Estudos Tectônicos (INCT-ET) network, consists of 7 broadband stations and 22 short-period stations. The broadband stations were arranged along an approximately 1000 km-long line with interstation spacing of about 100 km. They were equipped with STS-2.5 Streckheisen sensors and Q330 data loggers (24-bit) sampling at 100 Hz. The 22 short-period stations were equipped with L4A-3D Sercel sensors (2 Hz cut-off frequency) and 24-bit RT-130 digitizers sampling at 100 Hz. They were in operations between 2011 and 2012 and recorded continuously between 6 months and 1.5 years. The INCT-ET network was funded by the Conselho Nacional de Desenvolvimento Científico e Tecnológico (CNPq). Up to 6 broadband stations operated during 2007–2009 under the Institutos do Milênio project. These stations were equipped with KS2000 Geotech sensors and Geotech digitizers sampling continuously at 100 Hz. They recorded continuously for periods ranging from 6 months to 2 years, with two of them still in operation. This network was also funded by CNPq. Station RCBR belongs to the Global Seismographic Network (GSN). This station has been recording since 03/1999 with a CMG-3T Guralp sensor, which was replaced in 07/2004 by a STS-2 Streckeisen sensor, always feeding a Q330 data logger and sampling continuously at 40 Hz. Seven broadband stations belonging to the broader Brazilian Lithosphere Seismic Project (BLSP) (Assumpção et al., 2004) operated for 1.5 to 3.0 years in NE Brazil. They were equipped with either CMG-3T Guralp or STS-2 Streckeisen sensors and 24-bit RT-130 digitizers sampling at 100 Hz. Finally, 11 broadband stations deployed under the BOrborema Deep Electromagnetic and Seismic (BODES) experiment

were installed along an approximately NS line crossing the Araripe basin. They were equipped with RefTek 151-120 sensors and RT-130 digitizers. The stations were in operation between 2015 and 2017 and recorded continuously for ∼2 years at 100 Hz. Further detail on the 75 seismic stations is given in the Table S1 and their geographical location displayed in Figure 2.

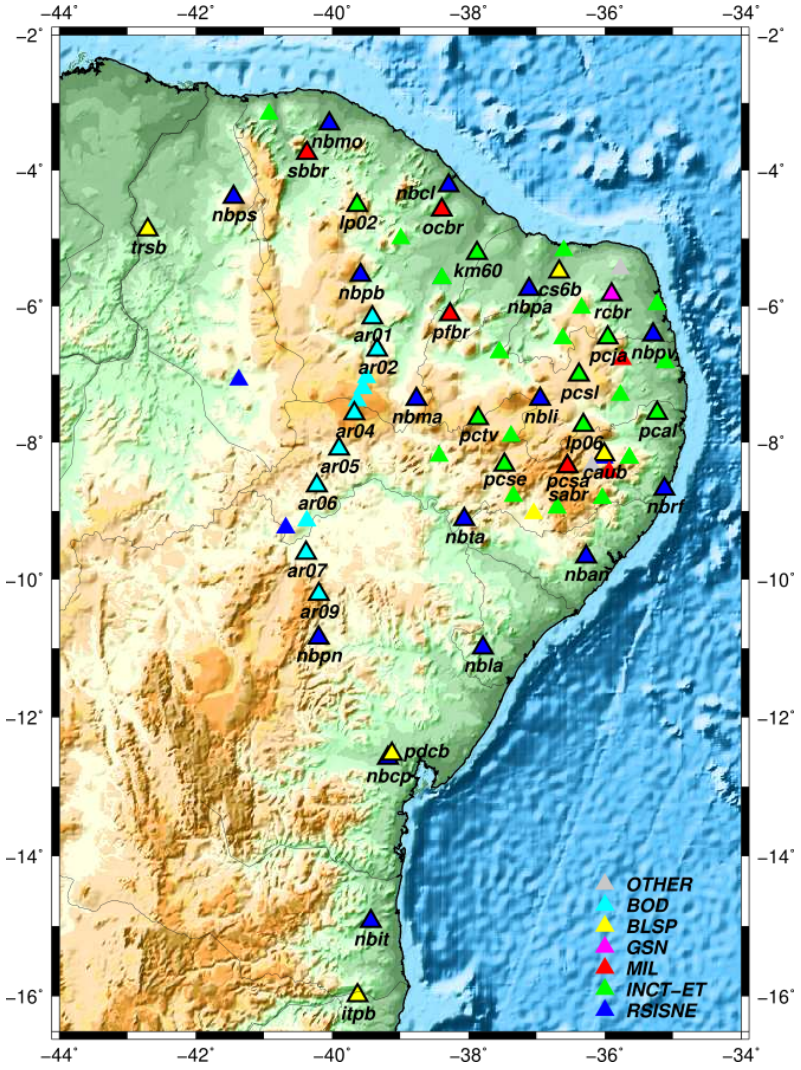

Figure 2. Topographic map of northeast Brazil with locations of broadband and short-period stations considered in this study. Stations were color-coded by network: stations from the network RSISNE are represented in dark blue, INCT-ET in green, Milenio in red, GSN in pink, BLSP in yellow, Bodes in light blue and others networks in grey (see legend). Only the selected stations have been named and are represented with black contour.

3.2 Receiver function processing and migration

Receiver functions were computed for the 75 stations making the combined network for northeast Brazil. Most of the receiver function estimates were developed by Luz et al. (2015a) in order to investigate lateral variations in crustal thickness and bulk Vp/Vs ratio across the Borborema Province. This dataset was later utilized by Almeida et al. (2015) to study the crustal architecture of the region from receiver function Common Conversion Point (CCP) stacks. We developed 1400 new receiver functions estimates at 11 temporary stations from the BODES network, following the same procedure as Luz et al. (2015a). The receiver function approach aims at retrieving P-to-S converted phases within the coda of teleseismic P waves that result from the interaction of the teleseismic P-wavefront with crustal and upper mantle discontinuities under the recording station (Langston, 1979, 1977) in order to produce estimates of the depth of the discontinuities. The converted phases are detected by deconvolving the radial and tangential components of the teleseismic waveforms by the corresponding vertical component (Ammon, 1991). This operation removes the effects of the source time function, near source propagation and instrumental response from the seismograms, leaving the signature of propagation local to the receiver.

The main processing steps involved in the development of the receiver function estimates are summarized below, and further details about computational and quality control procedures can be found in Luz et al. (2015a). First, we selected seismic sources with magnitude greater than 5.0 mb and occurring at epicentral distances between 30° and 90° from the selected stations (see Figure 3). The corresponding waveforms were then windowed 10 s before and 110 s after the P-wave arrival time, demeaned, detrended, tapered with a 5% cosine taper, and high-pass filtered above 0.05 Hz to remove low-frequency noise. All waveforms were re-sampled to 20 Hz, after low-pass filtering below 8 Hz to avoid aliasing. Before deconvolution, the waveforms were additionally low-pass filtered below 1.25 Hz with an acausal Gaussian filter (Gaussian width 2.5). The deconvolution procedure of the vertical component from the radial and transverse components was implemented through the iterative, time-domain procedure of Ligorria and Ammon (1999), with 500 iterations. The deconvolved time series were again filtered with the same Gaussian filter of width 2.5. Percent recoveries of the observed radial component under 85% were automatically rejected and the remaining receiver functions were visually inspected for each station to identify and remove outliers.

Prior to implementing the anisotropy analysis, each radial and tangential receiver function was migrated to depth after P to S ray-tracing through the global velocity model ak135-f (Kennett et al., 1995; Montagner and Kennett, 1996). The purpose of the migration is to correct the phase move-out introduced by varying incidence angles among the incoming teleseismic P-wavefronts, effectively equalizing the receiver function waveforms in the depth domain (Dueker and Sheehan, 1997). Migration before harmonic stripping at individual stations was previously utilized by Audet (2015); Cossette et al. (2016); Tarayoun et al. (2017). Similarly, Bianchi et al. (2010); Piana Agostinetti et al. (2011); Piana Agostinetti and Miller (2014) applied harmonic decomposition on depth-migrated cross-sections obtained through CCP stacking of receiver functions. Next, the migrated radial and transverse receiver functions for each station were grouped by back-azimuth in 36 non-overlapping, 10° wide bins, and averaged within each bin. A given station was then selected if it presented two averaged receiver functions (one radial and one tangential) in at least 9 bins. This selection criterion ensured a sampling of at least 90° in back-azimuth, either continuously or discontinuously, around the station. A back-azimuthal coverage from at least 9 bins (each 10°wide) allows the mapping

of either half the period for a 2-lobed pattern (anisotropy with plunging fast axis of symmetry) or a full period for a 4-lobed pattern (anisotropy with horizontal fast axis of symmetry). A total of 39 stations were thus selected for anisotropy analysis. An example of stacked and migrated receiver functions is displayed in Figure 4.

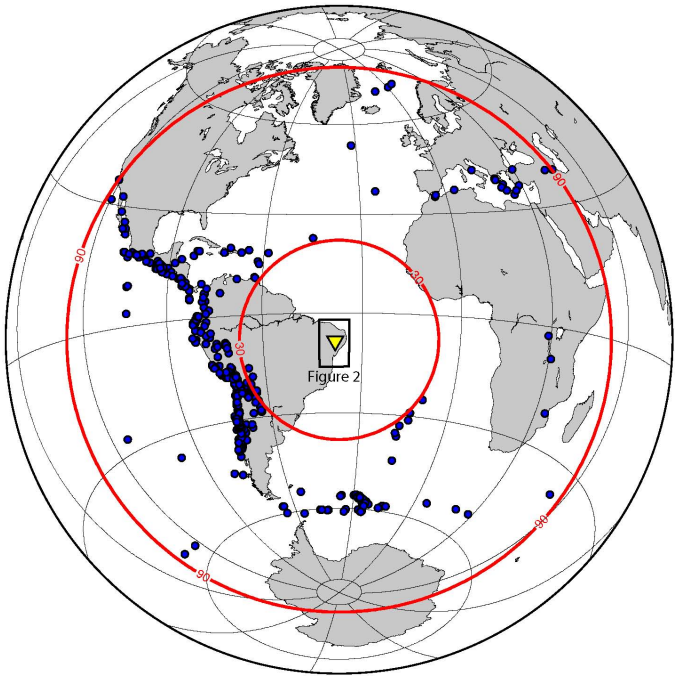

Figure 3. Location of earthquakes (blue circles) used for receiver function analyses, occurring at epicentral distances between 30°and 90°(red lines) and with magnitude $Mb \geq 5.0$.. The yellow triangle corresponds to the seismic network presented in Figure 2.

3.3 Estimating depth-dependent anisotropy within the lithosphere

In order to map deformation within the lithosphere, we estimate seismic anisotropy from the harmonic decomposition of receiver functions. The harmonic stripping method is described in Shiomi and Park (2008); Bianchi et al. (2010); Audet (2015). The method assumes that, at every depth, an ensemble of receiver functions can be expressed as a linear combination of $\cos(k\phi)$ and $\sin(k\phi)$ terms, where k is the harmonic degree or order, and ϕ is the back-azimuth. Shiomi and Park (2008) show that, for anisotropic media, radial and tangential receiver functions display a $\pi/2k$ shift for both $k = 1$ and $k = 2$ harmonic degrees; the tangential receiver functions can thus be added to the radial component after applying a phase shift of $+\pi/2k$ and naturally improve the azimuthal coverage around the station. After the harmonic decomposition is performed, up to 5 coefficient functions, corresponding to the first three harmonics, are obtained ($k = 0, 1, 2$). The first harmonic ($k = 0$) represents the isotropic variations from flat interfaces in an equivalent isotropic medium; for this harmonic, the signal is only presents in the radial component. If anisotropic structures are present at depth, the second and third harmonics ($k = 1$ and $k = 2$) contain energy with periodicity of $2\pi/k$. For $k = 1$, a two-lobed periodicity of 2π is either related to the presence of a dipping interface

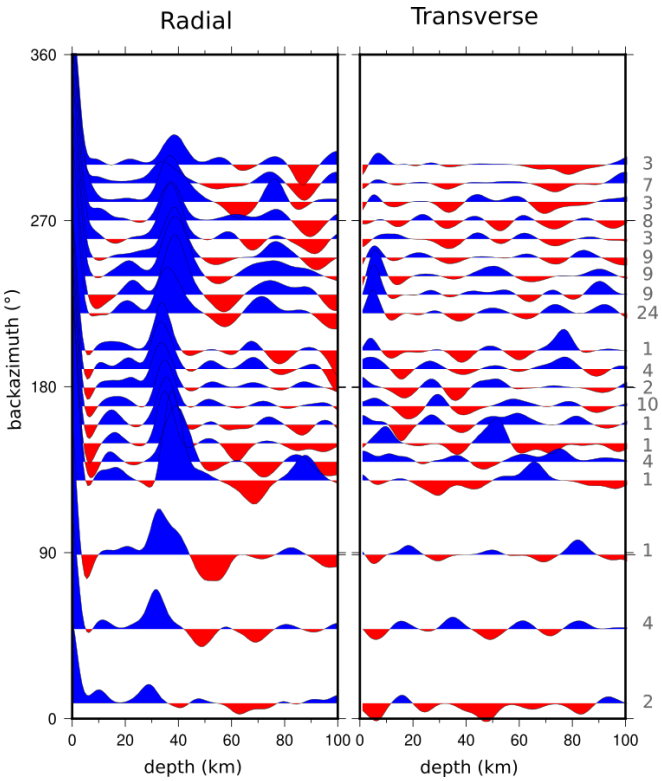

Figure 4. Example of stacked receiver functions represented by backazimuth bins of 10°at station PFBR. Grey numbers correspond to the number of stacked receiver functions.)

or to an anisotropic layer with a plunging symmetry axis (Maupin and Park, 2007). Two coefficient functions express the projection of this harmonic along the N-S and E-W directions, which correspond to the coefficients multiplying the $\cos(\phi)$ and $\sin(\phi)$ terms, respectively. For $k = 2$, a four-lobed periodicity of π is related to the presence of an anisotropic layer with a horizontal symmetry axis (Maupin and Park, 2007). As for the second degree harmonic, two coefficient functions express the projection of this harmonic degree along the N-S and 45°N directions, corresponding to the coefficients multiplying the $\cos(2\phi)$ and $\sin(2\phi)$ terms, respectively. The harmonic decomposition can be expressed in matrix form (eq. 1) and solved for the 5 coefficients for the 3 harmonic degrees ($k = 0, 1, 2$) through a singular value decomposition. These harmonics are calculated for every depth within a selected depth-window.

The matrix equation that implements the harmonic decomposition is given by

$$\begin{bmatrix} R_1(z) \\ \vdots \\ R_n(z) \\ T_1(z) \\ \vdots \\ T_n(z) \end{bmatrix} = \begin{bmatrix} 1 & \cos(\phi_1) & \sin(\phi_1) & \cos(2\phi_1) & \sin(2\phi_1) \\ \vdots & \vdots & \vdots & \vdots & \vdots \\ 1 & \cos(\phi_n) & \sin(\phi_n) & \cos(2\phi_n) & \sin(2\phi_n) \\ 0 & \cos(\phi_1+\pi/2) & \sin(\phi_1+\pi/2) & \cos(2(\phi_1+\pi/4)) & \sin(2(\phi_1+\pi/4)) \\ \vdots & \vdots & \vdots & \vdots & \vdots \\ 0 & \cos(\phi_n+\pi/2) & \sin(\phi_n+\pi/2) & \cos(2(\phi_n+\pi/4)) & \sin(2(\phi_n+\pi/4)) \end{bmatrix} * \begin{bmatrix} A(z) \\ B(z) \\ C(z) \\ D(z) \\ E(z) \end{bmatrix} \quad (1)$$

where ϕ_i is the back-azimuth of the i-th R (radial) and T (tangential) receiver function doublet, $A(z)$ represents the first harmonic coefficient ($k = 0$), $B(z)$ and $C(z)$ are the coefficient functions of the second harmonic ($k = 1$), and $D(z)$ and $E(z)$ are the coefficient functions of the third ($k = 2$) harmonic.

After solving the matrix equation (1) within a specific depth-window and calculating the five harmonic coefficients, we search for the presence of anisotropy by inspecting the $B(z)$, $C(z)$, $D(z)$ and/or $E(z)$ terms. If at least one of these component displays non-zero amplitudes, we calculate the energy of the second ($k = 1$) and the third ($k = 2$) harmonic degrees as proposed by Licciardi and Piana Agostinetti (2016):

$$E_{k=1} = \sum_{z=1}^{n} (B(z)^2 + C(z)^2) \quad (2)$$

and

$$E_{k=2} = \sum_{z=1}^{n} (D(z)^2 + E(z)^2) \quad (3)$$

These energy functions allow to discriminate between dipping interfaces/a plunging axis of symmetry and horizontal anisotropy. If $E_{k=1} > E_{k=2}$, the dominant anisotropy is either a dipping interface or an anisotropic layer with a plunging axis of symmetry. In that case, we rotate $B(z)$ and $C(z)$ in discrete back-azimuth increments α (where $\alpha \in [0, 2\pi]$) and search for the value of α that maximizes $B(z)$ (and therefore minimizes $C(z)$). This value of α can be directly interpreted as either the trend of the dip, in the case of dipping interface, or as the trend of the fast axis of symmetry in the case of plunging axis of symmetry. If $E_{k=2} > E_{k=1}$, the dominant anisotropy is an anisotropic layer with a horizontal axis of symmetry. In that case, we rotate $D(z)$ and $E(z)$ for each angle increment α (where $\alpha \in [0, 2\pi]$) and search for the value of α that maximizes $D(z)$ (and therefore minimizes $E(z)$). This value of α can be directly interpreted as the trend of either the fast or the slow axis of symmetry.

An example of harmonic decomposition is shown for station PFBR in Figure 5. In order to estimate uncertainties, we applied a bootstrap statistical approach by randomly re-sampling with replacement our receiver functions. We performed such analysis with 200 replications at each of the selected stations. From these 200 values, we estimated the standard error (2σ), which corresponds to the uncertainty in the direction of the fast-axis of symmetry. A measurement is considered as not reliable, and then rejected, if the estimated uncertainties are larger than 20°.

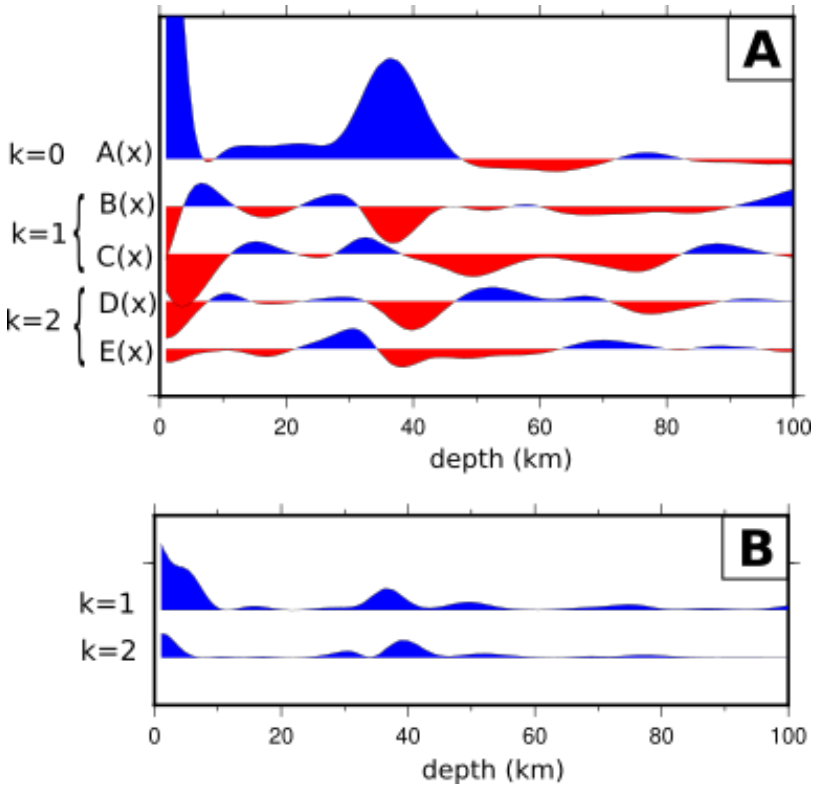

Figure 5. Example of results obtained at station PFBR with the harmonic stripping method of Bianchi et al. (2010). A/ From top to bottom are represented the harmonic functions obtained by solving the equation 1: $A(z)$ (first harmonic degree ($k = 0$), $B(z)$ ($\cos(\phi)$ term of the second degree harmonic ($k = 1$)), $C(z)$ ($\sin(\phi)$ term of the second degree harmonic ($k = 1$), $D(z)$ ($\cos(2\phi)$ term of the third ($k = 2$) harmonics), and, $E(z)$ ($\sin(2\phi)$ term of the third ($k = 2$) harmonics). B/ The energy is represented for harmonic degrees k=1 and k=2

4 Results

Anisotropy parameters were examined for each station at two depth-window ranges: (1) crust (Figure 6A), which was assumed to be located between 0 and 33 km depth, in agreement with the 32-40 km range estimated by Luz et al. (2015b) under the Borborema Plateau and 30-33 km under the surrounding basins; and (2) lithospheric mantle, which was taken to be between 33 and 100 km depth (Figure 6B). We assume that the layer with the strongest anisotropy will dominate the results in the case of several anisotropic layers. However, it might happen that results reflect the average value from different anisotropic layers, or from different types of anisotropy in the case of similar anisotropic strength. All results are indicated in Table 1.

An inspection of Figure 6A reveals that the crust of northeast Brazil presents seismic anisotropy, both within the interior of the continent and along the coast. A number of stations, however, display uncertainties larger than 20°. The significance of these large uncertainties are discussed in section 5. Unresolved anisotropic directions within the crust are recorded around longitude -40° for stations nbpb, ar02, ar05, ar06, nbpn, at the border of the Borborema Plateau (stations nbta, pctv, nbli, caub),

and within the Sergipe-Alagoas and Pernambuco basins (stations nban and pcal). The majority of stations that sample clear anisotropic directions display a NE-SW to E-W trending axis of symmetry, except stations cs6b (trend $\sim$ NNW-SSE), km60 and nbma (trends N-S). We mainly measure anisotropy with 2π-periodicity (k=1) related to a dipping interface or anisotropy with a plunging axis of symmetry, but some stations display clear π-periodic horizontal anisotropy (stations ar09, sabr, pcsa, pcsl, pcja, lp06, nbmo). ~~Realize that~~We note that, in most cases, even though k=1 harmonics display higher energy contents than k=2 harmonics, both pairs of harmonics display energies with comparable strengths (see supplementary materials, Figure S1). For example, station PFBR (Figure 5) shows clear, non-zero energy levels for both k=1 and k=2 harmonics in the crust between 0 and 33 km.

Figure 6B shows that the lithospheric mantle is characterized by seismic anisotropy throughout the entire Province, with the exception of a few stations that display large uncertainties (discussed in section 5). Those include stations within the Parnaíba basin (trsb), around longitude -40° (ar01, ao05 and nbpn), along the southern portion of the Borborema Plateau (nbta and pcse), and along a NE-SW axis located northwest of the Borborema Plateau (nbma, pfbr, nbpa, cs6b). Most anisotropic directions trend NE-SW to E-W, with the exception of stations km60 and nbma that show N-S trends. As for the crust, we mainly measure anisotropy with 2π-periodicity (k=1) related to a dipping interface or anisotropy with a plunging axis of symmetry, but some stations display clear π-periodic horizontal anisotropy (stations ar02, km60, lp06, pcal, nban, nbmo, nbpb, pctv, rcbr). Note that stations located along the continental margin show anisotropy within the lithospheric mantle with a fast axis of symmetry that is oblique (stations nbmo, nbpv, nbrf, nban, nbit) or perpendicular (stations nbcl, pcal) to the coast.

In the case where stations recorded anisotropic directions at both crustal and ~~mantellic~~mantle levels, most of them show consistent orientations in the two domains. There are a few instances, nonetheless, in which unaligned orientations for the crust and the lithospheric mantle are observed (ar04, ar09, nbcl, nbit, nbps, nbrf and rcbr).

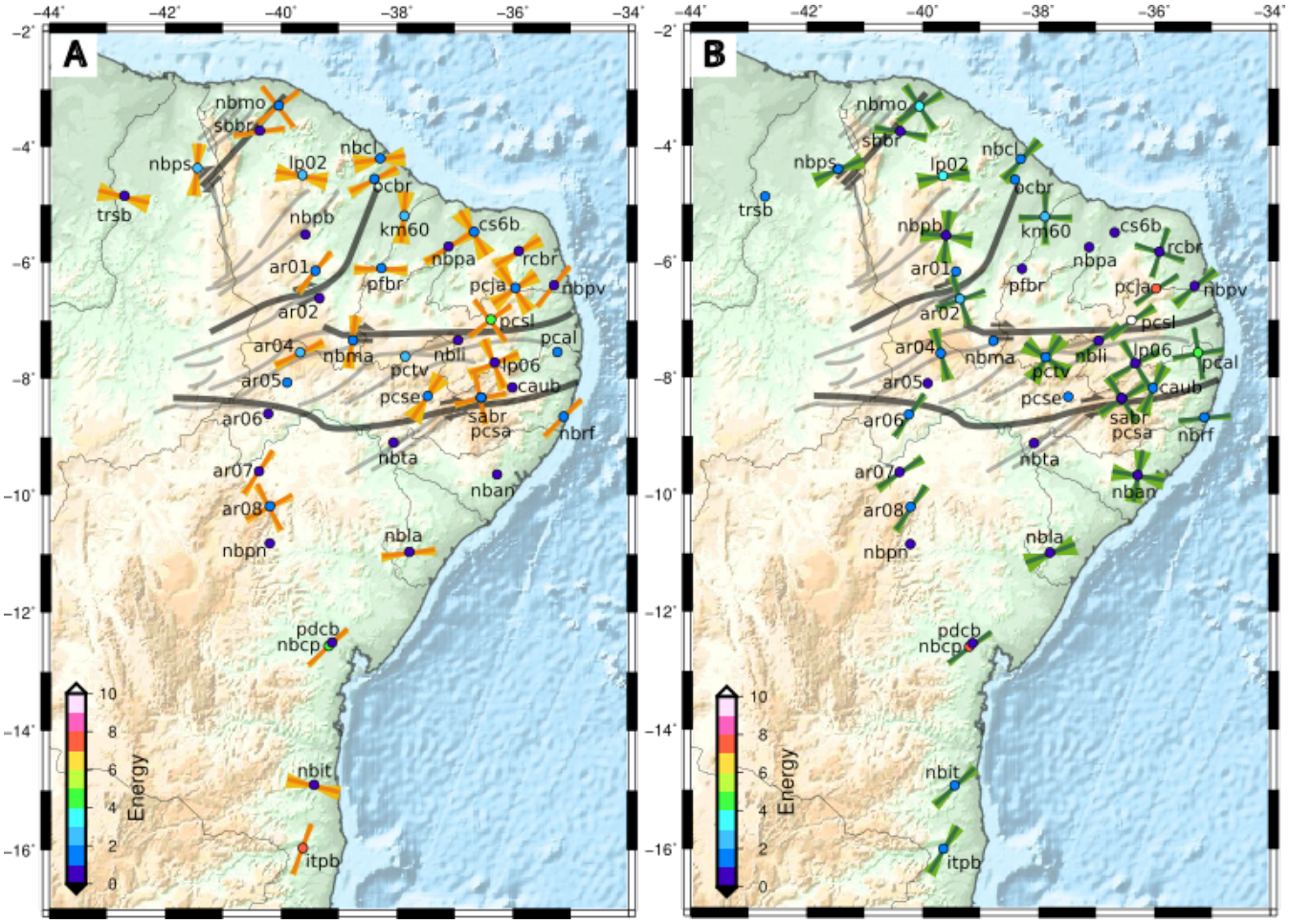

Figure 6. A) Map of symmetry directions (dark ~~sticks~~lines) obtained for the crust (0-32 km). When one ~~stick~~line is plotted at the station, it represents either the trend of the dip in the case of dipping interface or the trend of the fast axis in the case of plunging anisotropy. When two lines are plotted, they refer to the fast axis and to its perpendicular direction in the case of horizontal anisotropy. Light colors represent 2σ uncertainties estimated from the bootstrap ~~quantification~~ (~~200 re-sampling per station~~after re-sampling 200 times). B) Same for the lithospheric mantle (32-100 km). Station symbols have been color-coded according to the energy level of the dominant harmonic degree.

Table 1. Results of anisotropic symmetry directions for several depths ranges: 0-32 km, 32-100 km and 0-100 km. One direction corresponds either to the trend of the dip in the case of dipping interface or to the trend of the fast axis in the case of plunging anisotropy. When two directions are indicated, they refer to the fast axis and to its perpendicular direction (horizontal anisotropy). Uncertainties were estimated from bootstrap quantification (200 re-sampling at every station).

Station	0-32 km	32-100 km	Station	0-32 km	32-100 km
ar01	40 ± 8	44 ± 20	nbpa	70 ± 8	-
ar02	-	$83.5\text{-}173.5 \pm 7$	nbpb	-	$84.5\text{-}174.5 \pm 12$
ar04	-	$47.5\text{-}137.5 \pm 6$	nbpn	83 ± 8	$14.5\text{-}104.5 \pm 8$
ar05	-	$89\text{-}179 \pm 11$	nbps	13 ± 10	60 ± 20
ar06	-	30 ± 10	nbpv	40 ± 5	48 ± 9
ar07	36 ± 6	59 ± 10	nbrf	49 ± 6	82 ± 9
ar09	$66\text{-}156 \pm 5$	33 ± 14	nbta	$0\text{-}90 \pm 16$	-
caub	-	-	ocbr	74 ± 19	-
cs6b	155 ± 16	144 ± 17	pcal	150 ± 19	$84.5\text{-}174.5 \pm 5$
itpb	19 ± 5	71 ± 16	pcja	40 ± 19	54 ± 5
km60	10 ± 16	$2.5\text{-}92.5 \pm 5$	pcsa	$77\text{-}167 \pm 5$	74 ± 10
lp02	109 ± 20	-	pcse	-	$61.5\text{-}151.5 \pm 10$
lp06	-	$63\text{-}163 \pm 6$	pcsl	$53\text{-}143 \pm 5$	54 ± 10
nban	-	$10\text{-}100 \pm 17$	pctv	-	-
nbcl	84 ± 18	51 ± 8	pdcb	-	64 ± 10
nbcp	48 ± 5	56 ± 6	pfbr	94 ± 9	-
nbit	105 ± 10	47 ± 12	rcbr	60 ± 15	$15\text{-}105 \pm 5$
nbla	88 ± 6	$16\text{-}106 \pm 16$	sabr	-	$44.5\text{-}134.5 \pm 9$
nbli	-	49 ± 18	sbbr	82 ± 5	96 ± 14
nbma	6 ± 15	-	trsb	103 ± 20	$79\text{-}169 \pm 9$
nbmo	$52\text{-}142 \pm 6$	$56.5\text{-}146.5 \pm 7$			

5 Discussion

5.1 Pervasive anisotropy with (sub)horizontal fast axis of symmetry

As described is section 4, we observe in northeast Brazil a dominance of 2π-periodicity (k=1) anisotropy in the lithospheric mantle, which represents either a dipping interface or anisotropy with a plunging axis of symmetry. However, a close inspection of the energy of the k=2 harmonics also suggests an important contribution from anisotropy with a horizontal axis of symmetry. We were able to replicate this pattern with synthetic receiver functions by assuming anisotropy with a slightly (10 to 15°) dipping axis of symmetry (see supplementary materials, Figure S2). Note that, in that case, both k=1 and k=2 harmonics

display consistent orientations. This is, the orientation inferred from the k=1 harmonic degree is always parallel to one of the two orientations inferred from the k=2 harmonic degree.

Moreover, we noticed that the anisotropic fast axes of symmetry throughout the crust are consistent with those throughout the lithosphere for most of the stations, suggesting a prolongation of crustal structures within the lithospheric mantle. Within the continental interior, the anisotropic orientations are parallel or sub-parallel to the main E-W to NE-SW shear zone directions (stations ar02, nbli or lp06, for example). The consistency of the fast axis direction of lithospheric anisotropy with large structures observed at the surface suggest a continuation of the main shear zones into the lithospheric mantle, as suggested by Vauchez et al. (2012). A few exceptions, nonetheless, are observed for example at stations sabr, sbbr, and nbpb. Such discrepancies in the anisotropy orientations could be related to more local features such as fluid content, presence of cracks or plutonic bodies along the shear zones, fractures or mineral assemblages (Levin and Park, 1997; Mainprice and Nicolas, 1989).

5.2 Anisotropy along the passive margin

Inspection of stations located along the eastern and equatorial margins reveals that anisotropy exhibits - on average - directions either perpendicular or oblique to the coast in the lithospheric mantle. This observation is in agreement with SKS splitting measurements in this area performed by Bastow et al. (2011) and Assumpção et al. (2011). These authors concluded that the anisotropy reported from SKS splitting along the northeastern Brazilian margins must be related to fossil anisotropy inherited from the opening of the South Atlantic ocean. This interpretation is based on the relatively small time delay measured along the coast.

We compare the independent SKS splitting measurements with our results from harmonic stripping of receiver functions in Figure 7. For a better comparison we chose to represent the k=2 harmonics at stations where SKS splitting were measured because: (i) we expect only horizontal (recorded on the k=2 harmonics) or slightly dipping anisotropy in such geodynamical context; (ii) we observe in our data that k=1 and k=2 harmonics display energy within the same order of magnitude suggesting slightly dipping to horizontal anisotropy beneath most stations; and (iii) SKS waves are mainly ~~sensible~~sensitive to (sub)horizontal anisotropy (Levin et al., 2007). Figure 7 shows a good agreement between anisotropic orientations recorded by receiver functions and SKS-splitting along the eastern and equatorial margins, confirming that the recorded anisotropy beneath coastal stations is mainly located in the lithospheric mantle. The oblique to parallel orientation of anisotropy along the east and equatorial coasts, respectively, is consistent with the opening trend of the margin (Moulin et al., 2010).

5.3 ~~Asthenospheric flow heating the lithosphere~~Non-azimuthal anisotropy along the aborted Cariri-Potiguar rift

At a number of stations (ar05, nbma, pfbr, nbpa, cs6b), uncertainties for the direction of the fast axis of anisotropy are larger than 20°. ~~We think that anisotropy is just too small to be confidently retrieved, and interpret those stations as sampling an isotropic lithosphere.~~ These stations, however, display similar energy than stations with smaller uncertainties (see Figure 6 and supplementary material Figure S3).Interestingly, those stations seem to form a remarkable line trending NE-SW that approximately coincides with the location of the Cariri-Potiguar trend. Stations nbta and pcse also seem to align along the same direction more to the East.

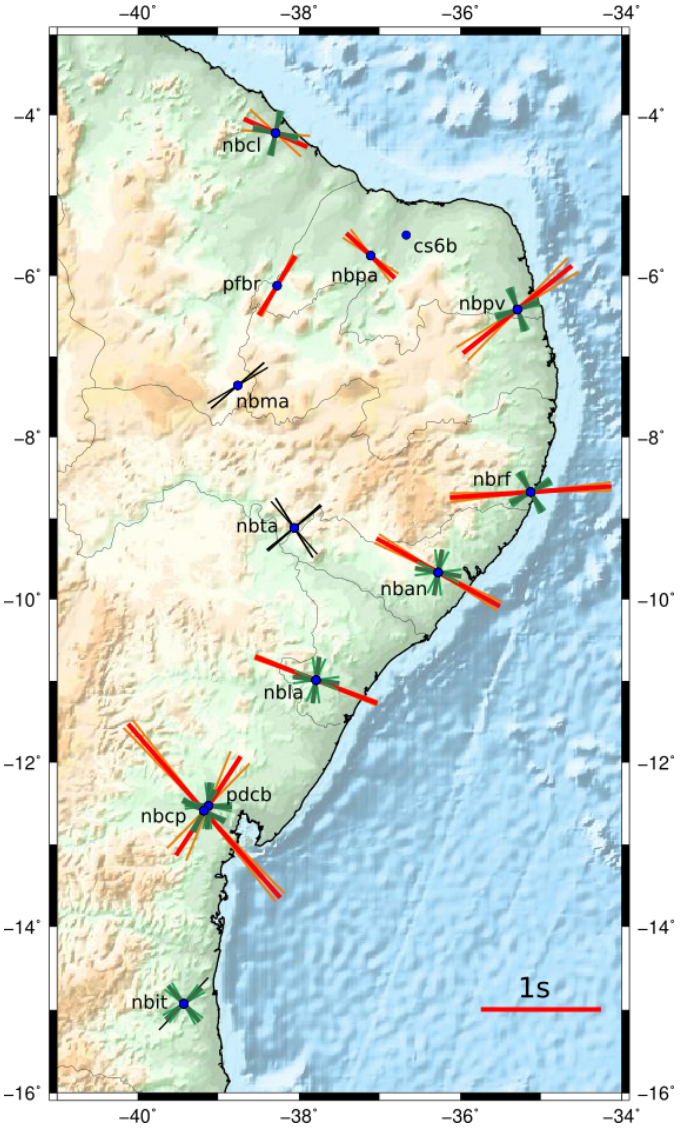

Figure 7. Comparison between fast axis of symmetry recorded by SKS-waves (red lines) and k=2 harmonics (green lines). SKS-splitting results are from Bastow et al. (2011) and Assumpção et al. (2011). Red arrows refer to mean fast axis orientation (arrow direction) and delay time (arrow size) beneath the station. When SKS measurements provides only null measurements, we display black lines which are on the direction of the back-azimuth of the recorded event.

~~One explanation for the absence of lithospheric-scale anisotropy could be the destruction of anisotropic fabrics through sub-lithospheric heating of the overlying lithosphere. This hypothesis was proposed for the Cameroon Volcanic Line (CVL) by Deplaen et al. (2014), who argued that hotspot tectonism associated with the Mesozoic opening of the South Atlantic may have thermomechanically eroded Precambrian age fossil lithospheric fabrics beneath the CVL. Indeed, the presence of relatively~~

~~shallow asthenosphere north-west of the Borborema Plateau has been recently postulated from a P-wave tomography study of the Borborema Province (Simões Neto et al., 2019). These authors identified a NE-SW trending low-velocity channel bordering the Plateau that closely coincides with the observed isotropic alignment. Moreover, independent SKS splitting measurements performed at those stations by Bastow et al. (2015) reported either null measurements (stations nbma, cs6b, nbta) or really weak anisotropy (stations pfbr and nbpa).~~ This NE-SW oriented line is located above a NE-SW trending channel of thin lithosphere imaged by the tomographic study of Simões Neto et al. (2019). We suggest that deformation from thermo-mechanical erosion by horizontal, sub-lithospheric flow along the channel - also postulated by Simões Neto et al. (2019) - must be ongoing above this NE-SW channel. Also, as initial thinning of the lithosphere along the channel was triggered by Mesozoic extension along the Cariri-Potiguar trend, alterations to the original Precambrian anisotropic fabric by Mesozoic extension might still be present. Additionally, we note that the location of the Cariri-Potiguar trend also marks the boundary between the EW striking shear zones in the southern Province from the NE-SW striking shear zones in the western Province (Figure 1). This suggests the Cariri-Potiguar trend also marks the location of a former paleo-suture that later acted as a zone of weakness along which the Mesozoic rift (now aborted) could develop. Thus, we believe the non-azimuthal anisotropy recorded at stations located along this trend is likely related to complex fossil anisotropic fabrics resulting from a combination of deformation along the ancient collision between Precambrian blocks, Mesozoic extension, and thermo-mechanical erosion/mantle dragging by sub-lithospheric flow.

6 Conclusions

We have investigated depth-dependent anisotropy in the Borborema Province of NE Brazil through harmonic decomposition of receiver functions developed at 39 stations in the region. Our main results include: (i) anisotropy within the Province is characterized by a horizontal to slightly dipping fast axis of symmetry; (ii) consistency of anisotropic orientations within the crust and the lithospheric mantle suggest a continuation of surface shear-zones down to lithospheric depths; (iii) fast axes of symmetry are oriented parallel to the main shear zones within the continental interior and sub-parallel to Mesozoic extension along the passive margins, consistent with a fossil origin inherited from the opening of the South Atlantic Ocean; (iv) absence of anisotropy along a NE-SW trending line in the center of the Province might be related to heating of the lithosphere by an asthenospheric channel identified in an independent tomography study.

Acknowledgements. Data used for this study were acquired due to funding from the national oil company Petrobras and the Conselho Nacional de Desenvolvimento Científico e Tecnológico (CNPq). GL was supported by a 1-year scholarship from the Programa Nacional de Pósdoutorado da Coordenação de Aperfeiçoamento de Pessoal de Nível Superior (PNPD/CAPES). This work was also supported by the "Laboratoire d'Excellence" LabexMer (ANR-10-LABX-19) and co-funded by a grant from the French government under the program "Investissements d'Avenir", and by a grant from the Regional Council of Brittany (SAD programme). JJ thanks the Conselho Nacional de Desenvolvimento Científico e Tecnológico (CNPq) for his research fellowship (CNPq, process no 304421/2015-4). We used the open-source

toolbox GMT v.5.4 (Wessel et al., 2013) to produce the figures. Thanks are due to Nicola Piana Agostinetti for constructive discussions about harmonic decomposition method, and to Andrea Tommasi for interesting debates on the tectonics of northeast Brazil.

References

Almeida, Y., Julià, J., and Frassetto, a.: Crustal architecture of the Borborema Province, NE Brazil, from receiver function CCP stacks: Implications for Mesozoic stretching and Cenozoic uplift, Tectonophysics, 649, 68–80, https://doi.org/10.1016/j.tecto.2015.03.001, http://linkinghub.elsevier.com/retrieve/pii/S0040195115001651, 2015.

Ammon, C. J.: The isolation of receiver effects from teleseismic P weveforms, Bulletin of the Seismological Society of America, 81, 2504–2510, 1991.

Araújo, C. E. G., Weinberg, R. F., and Cordani, U. G.: Extruding the Borborema Province (NE-Brazil): a two-stage Neoproterozoic collision process, Terra Nova, 26, 157–168, https://doi.org/10.1111/ter.12084, http://doi.wiley.com/10.1111/ter.12084, 2014.

Arthaud, M. H., Caby, R., Fuck, R. A., Dantas, E. L., and Parente, C. V.: Geology of the northern Borborema Province, NE Brazil and its correlation with Nigeria, NW Africa, Geological Society, London, Special Publications, 294, 49–67, 2008.

Assine, M. L.: Bacia do Araripe, Boletim de Geociências da PETROBRAS, 15, 371–389, 2007.

Assumpção, M., Feng, M., Mandel, E., Barbosa, J. R., Bianchi, M., van der Lee, S., Marone, F., and van der Meijde, M.: BLSP02: Projeto de estudo sismologico da crosta e manto superior no Brasil, in: Simposio Regional da Sociedad Brasileira de Geofisica, Sao Paulo, Brazil, 2004.

Assumpção, M., Guarido, M., Lee, S. v. d., and Dourado, J. C.: Upper-mantle seismic anisotropy from SKS splitting in the South American stable platform: A test of asthenospheric flow models beneath the lithosphere, Lithosphere, 3, 173–180, https://doi.org/10.1130/L99.1, https://pubs.geoscienceworld.org/gsa/lithosphere/article/3/2/173/145585/upper-mantle-seismic-anisotropy-from-sks-splitting, 2011.

Audet, P.: Layered crustal anisotropy around the San Andreas Fault near Parkfield, California, Journal of Geophysical Research: Solid Earth, 120, 3527–3543, https://doi.org/10.1002/2014JB011821, http://doi.wiley.com/10.1002/2014JB011821, 2015.

Bastow, I., Julia, J., Nascimento, A., Fuck, R., and Buckthorp, T.: Upper mantle anisotropy of the Borborema Province , NE Brazil : Implications for intra-plate deformation and sub-cratonic asthenospheric flow, Tectonophysics, https://doi.org/10.1016/j.tecto.2015.06.024, http://dx.doi.org/10.1016/j.tecto.2015.06.024, 2015.

Bastow, I. D., Thompson, D. a., Wookey, J., Kendall, J. M., Helffrich, G., Snyder, D. B., Eaton, D. W., and Darbyshire, F. a.: Precambrian plate tectonics: Seismic evidence from Northern Hudson Bay, Canada, Geology, 39, 91–94, https://doi.org/10.1130/G31396.1, 2011.

Bianchi, I., Park, J., Piana Agostinetti, N., and Levin, V.: Mapping seismic anisotropy using harmonic decomposition of receiver functions: An application to Northern Apennines, Italy, Journal of Geophysical Research, 115, B12 317, https://doi.org/10.1029/2009JB007061, http://doi.wiley.com/10.1029/2009JB007061, 2010.

Cordani, U. G., D'Agrella-Filho, M. S., Brito-Neves, B. B., and Trindade, R. I. F.: Tearing up Rodinia: The neoproterozoic palaeogeography of South American cratonic fragments, Terra Nova, 15, 350–359, https://doi.org/10.1046/j.1365-3121.2003.00506.x, 2003.

Cossette, E., Audet, P., Schneider, D., and Grasemann, B.: Structure and anisotropy of the crust in the Cyclades, Greece, using receiver functions constrained by in situ rock textural data, Journal of Geophysical Research: Solid Earth, 121, 2661–2678, https://doi.org/10.1002/2015JB012460, https://agupubs.onlinelibrary.wiley.com/doi/full/10.1002/2015JB012460, 2016.

da Nóbrega, M. A., Sá, J. M., Bezerra, F. H. R., Hadler Neto, J. C., Lunes, P. J., Guedes, S., Tello Saenz, C. A., Hackspacher, P. C., and Lima-Filho, F. P.: The use of apatite fission track thermochronology to constrain fault movements and sedimentary basin evolution in northeastern Brazil, Radiation Measurements, 39, 627–633, https://www.sciencedirect.com/science/article/pii/S1350448704002690, 2005.

de Matos, R. M. D.: The Northeast Brazilian Rift System, Tectonics, 11, 766–791, 1992.

de Oliveira, R. G. and Medeiros, W. E.: Evidences of buried loads in the base of the crust of Borborema Plateau (NE Brazil) from Bouguer admittance estimates, Journal of South American Earth Sciences, 37, 60–76, https://doi.org/10.1016/j.jsames.2012.02.004, http://dx.doi.org/10.1016/j.jsames.2012.02.004, 2012.

Deplaen, R. S. M., Bastow, I. D., Chambers, E. L., Keir, D., Gallacher, R. J., and Keane, J.: The development of magmatism along the Cameroon Volcanic Line: Evidence from seismicity and seismic anisotropy, Journal of Geophysical Research: Solid Earth, 119, 4233–4252, https://doi.org/10.1002/2013JB010583, 2014.

Dias, R. C., Julià, J., and Schimmel, M.: Rayleigh-Wave, Group-Velocity Tomography of the Borborema Province, NE Brazil, from Ambient Seismic Noise, Pure and Applied Geophysics, https://doi.org/10.1007/s00024-014-0982-9, 2014.

Dueker, K. G. and Sheehan, A. F.: Mantle discontinuity structure from midpoint stacks of converted P to S waves across the Yellowstone hotspot track, Journal of Geophysical Research, 102, 8313, https://doi.org/10.1029/96JB03857, http://doi.wiley.com/10.1029/96JB03857, 1997.

Garcia, X., Julià, J., Nemocón, A. M., and Neukirch, M.: Lithospheric thinning under the Araripe Basin (NE Brazil) from a long-period magnetotelluric survey: Constraints for tectonic inversion, Gondwana Research, 68, 174–184, https://doi.org/10.1016/j.gr.2018.11.013, http://www.sciencedirect.com/science/article/pii/S1342937X19300024, 2019.

Jardim de Sá, E. F., Macedo, M. H. F., Fuck, R. A., and Kawashita, K.: Terrenos proterozóicos na Província Borborema e a margem norte do Cráton São Francisco, Revista Brasileira de Geociências, 22, 472–480, 1992.

Kennett, B. L. N., Engdah, E. R., and Buland, R.: Constraints on seismic velocities in the Earth from traveltimes, Geophysical Journal International, 122, 108–124, 1995.

Kirkpatrick, J. D., Bezerra, F. H. R., Shipton, Z. K., do Nascimento, A. F., Pytharouli, S. I., Lunn, R. J., and Soden, A. M.: Scale-dependent influence of pre-existing basement shear zones on rift faulting: a case study from NE Brazil, Journal of the Geological Society, 170, 237–247, https://doi.org/10.1144/jgs2012-043.Scale-dependent, 2013.

Knesel, K. M., Souza, Z. S., Vasconcelos, P. M., Cohen, B. E., and Silveira, F. V.: Young volcanism in the Borborema Province, NE Brazil, shows no evidence for a trace of the Fernando de Noronha plume on the continent, Earth and Planetary Science Letters, 302, 38–50, https://doi.org/10.1016/j.epsl.2010.11.036, http://dx.doi.org/10.1016/j.epsl.2010.11.036, 2011.

Langston, C. A.: Corvallis, Oregon, Crustal and upper mantle receiver structure from teleseismic P and S waves, Bulletin of the Seismological Society of America, 67, 713–724, 1977.

Langston, C. A.: Structure Under Mount Rainier, washington, Inffered from Teleseismic Body Waves, Journal of Geophysical Research, 84, 4749–4762, 1979.

Levin, V. and Park, J.: Crustal anisotropy in the Ural Mountains foredeep from teleseismic receiver functions, Geophysical Research Letters, 24, 1283–1286, 1997.

Levin, V., Okaya, D., and Park, J.: Shear wave birefringence in wedge-shaped anisotropic regions, Geophysical Journal International, 168, 275–286, https://doi.org/10.1111/j.1365-246X.2006.03224.x, https://academic.oup.com/gji/article-lookup/doi/10.1111/j.1365-246X.2006.03224.x, 2007.

Licciardi, A. and Piana Agostinetti, N.: A semi-automated method for the detection of seismic anisotropy at depth via receiver function analysis, Geophysical Journal International, 205, 1589–1612, https://doi.org/10.1093/gji/ggw091, https://academic.oup.com/gji/article/205/3/1589/654451, 2016.

Ligorria, P. and Ammon, C. J.: Iterative Deconvolution and Receiver-Function Estimation, Bulletin of the Seismological Society of America, 89, 1395–1400, 1999.

Lima Neto, H. C., Ferreira, J. M., Bezerra, F. H. R., Assumpção, M. S., do Nascimento, A. F., Sousa, M. O., and a.S. Menezes, E.: Upper crustal earthquake swarms in São Caetano: Reactivation of the Pernambuco shear zone and trending branches in intraplate Brazil, Tectonophysics, 608, 804–811, https://doi.org/10.1016/j.tecto.2013.08.001, http://linkinghub.elsevier.com/retrieve/pii/S0040195113004800, 2013.

Luz, R. M. N., Julià, J., and Nascimento, A. F.: Bulk crustal properties of the Borborema Province , NE Brazil , from P-wave receiver functions : Implications for models of intraplate Cenozoic uplift, Tectonophysics, 644-645, 81–91, https://doi.org/10.1016/j.tecto.2014.12.017, http://dx.doi.org/10.1016/j.tecto.2014.12.017, 2015a.

Luz, R. M. N., Julià, J., and Nascimento, A. F.: Crustal structure of the eastern Borborema Province, NE Brazil, from the joint inversion of receiver functions and surface-wave dispersion: Implications for plateau uplift ., Journal of Geophysical Research : Solid Earth, 120, 3848–3869, https://doi.org/10.1002/2015JB011872, 2015b.

Mainprice, D. and Nicolas, A.: Development of shape and lattice preferred orientations: application to the seismic anisotropy of the lower crust, Journal of Structural Geology, 11, 175–189, https://doi.org/10.1016/0191-8141(89)90042-4, http://linkinghub.elsevier.com/retrieve/pii/0191814189900424, 1989.

Marques, F. O., Nogueira, F. C. C., Bezerra, F. H. R., and de Castro, D. L.: The Araripe Basin in NE Brazil: An intracontinental graben inverted to a high-standing horst, Tectonophysics, 630, 251–264, https://doi.org/10.1016/j.tecto.2014.05.029, http://www.sciencedirect.com/science/article/pii/S0040195114003023, 2014.

Maupin, V. and Park, J.: Seismology and Structure of the Earth: Theory and Observations - Wave propagation in anisotropic media, in: Treatise on Geophysics, Elsevier, pp. 289–321, Elsevier, Elsevier, elsevier edn., 2007.

Mizusaki, A., Thomaz-Filho, A., Milani, E., and de Césero, P.: Mesozoic and Cenozoic igneous activity and its tectonic control in northeastern Brazil, Journal of South American Earth Sciences, 15, 183–198, 2002.

Montagner, J.-P. and Kennett, B. L. N.: How to reconcile body-wave and normal-mode reference earth models, Geophysical Journal International, 125, 229–248, https://doi.org/10.1111/j.1365-246X.1996.tb06548.x, https://onlinelibrary.wiley.com/doi/abs/10.1111/j.1365-246X.1996.tb06548.x, 1996.

Morais Neto, J. M., Hegarty, K. a., Karner, G. D., and Alkmim, F. F.: Timing and mechanisms for the generation and modification of the anomalous topography of the Borborema Province, northeastern Brazil, Marine and Petroleum Geology, 26, 1070–1086, https://doi.org/10.1016/j.marpetgeo.2008.07.002, http://dx.doi.org/10.1016/j.marpetgeo.2008.07.002, 2009.

Moulin, M., Aslanian, D., and Unternehr, P.: A new starting point for the South and Equatorial Atlantic Ocean, Earth-Science Reviews, 98, 1–37, https://doi.org/10.1016/j.earscirev.2009.08.001, http://www.sciencedirect.com/science/article/pii/S0012825209001172, 2010.

Neves, S. P.: Proterozoic history of the Borborema province (NE Brazil): Correlations with neighboring cratons and Pan-African belts and implications for the evolution of western Gondwana, Tectonics, 22, https://doi.org/10.1029/2001TC001352, 2003.

Neves, S. P., Vauchez, A., and Feraud, G.: Tectono-thermal evolution, magma emplacement, and shear zone development in the Caruaru area (Borborema Province, NE Brazil), Precambrian Research, 99, 1–32, https://doi.org/10.1016/S0301-9268(99)00026-1, 2000.

Nogueira, F. C. C., Marques, F. O., Bezerra, F. H. R., de Castro, D. L., and Fuck, R. A.: Cretaceous intracontinental rifting and post-rift inversion in NE Brazil: Insights from the Rio do Peixe Basin, Tectonophysics, 644-645, 92–107, https://www.sciencedirect.com/science/article/pii/S0040195115000074, 2015.

Peulvast, J.-P. and Bétard, F.: A history of basin inversion, scarp retreat and shallow denudation: The Araripe basin as a keystone for understanding long-term landscape evolution in NE Brazil, Geomorphology, 233, 20–40, https://doi.org/10.1016/j.geomorph.2014.10.009, http://www.sciencedirect.com/science/article/pii/S0169555X1400511X, 2015.

Piana Agostinetti, N. and Miller, M. S.: The fate of the downgoing oceanic plate: Insight from the Northern Cascadia subduction zone, Earth and Planetary Science Letters, 408, 237–251, https://doi.org/10.1016/j.epsl.2014.10.016, http://www.sciencedirect.com/science/article/pii/S0012821X14006372, 2014.

Piana Agostinetti, N., Bianchi, I., Amato, A., and Chiarabba, C.: Fluid migration in continental subduction: The Northern Apennines case study, Earth and Planetary Science Letters, 302, 267–278, https://doi.org/10.1016/j.epsl.2010.10.039, http://www.sciencedirect.com/science/article/pii/S0012821X10006928, 2011.

Pinheiro, A. G. and Julia, J.: Normal thickness of the upper mantle transition zone in NE Brazil does not favour mantle plumes as origin for intraplate Cenozoic volcanism, Geophysical Journal International, 199, 996–1005, https://doi.org/10.1093/gji/ggu281, 2014.

Santos, A. C., Padilha, A. L., Fuck, R. A., Pires, A. C., Vitorello, I., and Pádua, M. B.: Deep structure of a stretched lithosphere: Magnetotelluric imaging of the southeastern Borborema province, NE Brazil, Tectonophysics, 610, 39–50, https://doi.org/10.1016/j.tecto.2013.10.008, http://www.sciencedirect.com/science/article/pii/S0040195113006124, 2014.

Shiomi, K. and Park, J.: Structural features of the subducting slab beneath the Kii Peninsula, central Japan: Seismic evidence of slab segmentation, dehydration, and anisotropy, Journal of Geophysical Research: Solid Earth, 113, 1–13, https://doi.org/10.1029/2007JB005535, 2008.

Simões Neto, F. L., Julià, J., and Schimmel, M.: Upper-mantle structure of the Borborema Province, NE Brazil, from P-wave tomography: implications for rheology and volcanism, Geophysical Journal International, 216, 231–250, https://doi.org/10.1093/gji/ggy421, https://academic.oup.com/gji/article/216/1/231/5127046, 2019.

Tarayoun, A., Audet, P., Mazzotti, S., and Ashoori, A.: Architecture of the crust and uppermost mantle in the northern Canadian Cordillera from receiver functions, Journal of Geophysical Research: Solid Earth, 122, 5268–5287, https://doi.org/10.1002/2017JB014284, https://agupubs.onlinelibrary.wiley.com/doi/full/10.1002/2017JB014284, 2017.

Tommasi, A. and Vauchez, A.: Continental rifting parallel to ancient collisional belts : an effect of the mechanical anisotropy of the lithospheric mantle, Earth and Planetary Science Letters, 185, 199–210, 2001.

Tommasi, A., Vauchez, A., and Daudré, B.: Initiation and propagation of shear zones in a heterogeneous continental lithosphere, Journal of Geophysical Research, 100, 22 083–22 101, 1995.

Van Schmus, W. R., Kozuch, M., and de Brito Neves, B. B.: Precambrian history of the Zona Transversal of the Borborema Province, NE Brazil: Insights from Sm-Nd and U-Pb geochronology, Journal of South American Earth Sciences, 31, 227–252, https://doi.org/10.1016/j.jsames.2011.02.010, http://linkinghub.elsevier.com/retrieve/pii/S0895981111000186, 2011.

Vauchez, A. and da Silva, M. E.: Termination of a continenta-scale strike-slip fault in partially melted crust: The West Pernambuco shear zone, northeast Brazil, Geology, 20, 1007–1010, https://doi.org/10.1130/0091-7613(1992)020<1007, 1992.

Vauchez, a., Neves, S., Caby, R., Corsini, M., Egydio-Silva, M., Arthaud, M., and Amaro, V.: The Borborema shear zone system, NE Brazil, Journal of South American Earth Sciences, 8, 247–266, https://doi.org/10.1016/0895-9811(95)00012-5, 1995.

Vauchez, A., Tommasi, A., and Mainprice, D.: Faults (shear zones) in the Earth's mantle, Tectonophysics, 558-559, 1–27, https://doi.org/10.1016/j.tecto.2012.06.006, http://linkinghub.elsevier.com/retrieve/pii/S0040195112003125, 2012.

Wessel, P., Smith, W. H., Scharroo, R., Luis, J., and Wobbe, F.: Generic Mapping Tools: Improved Version Released - Wessel - 2013 - Eos, Transactions American Geophysical Union - Wiley Online Library, https://agupubs.onlinelibrary.wiley.com/doi/abs/10.1002/2013EO450001, 2013.

Table S1 lists the seismic stations used in this study. We report station coordinates (latitude and longitude), elevation and recording time window. The last column indicates whether the station was selected for harmonic stripping or not (see details in section 3).

Table S1. List of stations with coordinates, elevation, recording time window, and selection

Station	Latitude °N	Longitude °E	Elevation (m)	Recording time window	Selection
RSISNE (Broadband Stations)					
nban	-9.669	-36.275	261	29/09/2011 - 25/11/2013	yes
nbca	-8.226	-36.013	616	09/04/2012 - 22/04/2013	no
nbcl	-4.224	-38.291	020	26/05/2011 - 28/12/2013	yes
nbcp	-12.589	-39.181	222	27/09/2011 - 30/04/2013	yes
nbit	-14.931	-39.434	178	13/10/2011 - 25/11/2013	yes
nbla	-10.993	-37.789	217	03/09/2011 - 25/11/2013	yes
nbli	-7.364	-36.950	613	18/07/2011 - 25/11/2013	yes
nbma	-7.365	-38.764	437	06/07/2011 - 25/11/2013	yes
nbmo	-3.311	-40.041	098	29/12/2010 - 28/12/2012	yes
nbpa	-5.750	-37.112	091	12/04/2011 - 25/11/2013	yes
nbpb	-5.543	-39.584	260	29/05/2011 - 28/12/2013	yes
nbpn	-10.847	-40.199	387	05/04/2011 - 25/11/2013	yes
nbps	-4.394	-41.446	719	24/09/2011 - 25/11/2013	yes
nbpv	-6.418	-35.291	092	30/04/2011 - 25/11/2013	yes
nbrf	-8.679	-35.127	061	02/08/2011 - 25/11/2013	yes
nbta	-9.122	-38.063	344	27/07/2011 - 25/11/2013	yes
nbjg	-5.5932	-38.3947	119	17/07/2013 - 25/11/2013	no
nbpe	-9.2465	-40.6804	450	12/08/2013 - 16/11/2013	no
nbpi	-7.083	-41.3699	247	12/08/2013 - 24/10/2013	no
INCT-ET					
Broadband Stations					
lp01	-3.167	-40.926	067	20/03/2012 - 06/02/2013	no
lp02	-4.513	-39.635	688	20/03/2012 - 06/02/2013	yes
lp03	-5.0056	-38.9935	234	2012.073 to 2013.030	no
lp04	-5.590	-38.386	138	28/05/2012 - 05/02/2013	no
lp05	-6.678	-37.546	248	04/02/2012 - 05/02/2013	no
lp06	-7.747	-36.315	522	25/03/2012 - 28/02/2013	yes
lp07	-8.227	-35.6401	531	25/03/2012 - 28/02/2013	no
Short-period Stations					
km60	-5.219	-37.876	141	03/10/2011 - 13/08/2012	yes
pcac	-6.475	-36.62	293	28/09/2011 - 24/04/2013	no

pcal	-7.569	-35.233	098	05/12/2011 - 23/04/2013	yes
pcbs	-7.747	-36.315	522	23/11/2011 - 19/03/2013	no
pccc	-6.026	-36.342	614	15/08/2012 - 13/04/2013	no
pccg	-7.305	-35.772	409	15/09/2011 - 24/04/2013	no
pcgr	-8.228	-35.640	522	22/11/2011 - 19/03/2013	no
pcgu	-7.906	-37.377	657	16/08/2012 - 16/05/2013	no
pcja	-6.463	-35.958	310	04/10/2011 - 24/04/2013	yes
pcjg	-5.593	-38.395	134	03/11/2011 - 19/03/2013	no
pcma	-5.181	-36.603	160	06/10/2011 - 07/06/2012	no
pcmn	-6.828	-35.114	036	25/11/2011 - 19/03/2013	no
pcpi	-5.976	-35.235	064	23/10/2011 - 14/08/2012	no
pcqp	-8.817	-36.037	549	15/08/2012 - 16/05/2013	no
pcsa	-8.351	-36.551	694	19/10/2011 - 24/04/2013	yes
pcse	-8.326	-37.473	482	07/12/2011 - 24/04/2013	yes
pcsl	-7.008	-36.381	596	06/12/2011 - 23/04/2013	yes
pcso	-8.957	-36.702	858	16/08/2012 - 16/05/2013	no
pcst	-8.199	-38.431	419	17/08/2012 - 16/05/2013	no
pctu	-8.785	-37.341	746	16/08/2012 - 16/05/2013	no
pctv	-7.646	-37.860	746	07/12/2011 - 25/04/2013	yes
pcvs	-6.679	-37.546	210	29/09/2011 - 25/03/2012	no
Milênio (Broadband Stations					
agbr	-8.4295	-35.9361	489	05/04/2007 - 01/03/2008	no
ocbr	-4.5813	-38.392	076	16/08/2007 - 04/07/2009	yes
pfbr	-6.1216	-38.271	120	26/08/2007 - 22/02/2013	yes
sabr	-8.3511	-36.550	681	17/04/2009 - 03/09/2011	yes
sbbr	-3.7451	-40.371	056	22/07/2007 - 07/06/2013	yes
slbr	-6.7815	-35.744	544	22/09/2007 - 16/10/2008	no
GSN (Broadband Station					
rcbr	-5.8274	-35.901	420	20/08/2007 - 30/12/2013	yes
BLSP (Broadband Stations					
agbl	-9.038	-37.045	448	07/02/2002 - 30/11/2004	no
caub	-8.176	-36.010	490	07/02/2002 - 30/11/2004	yes
crtb	-13.4321	-44.5819	541	22/12/2003 - 29/04/2004	no
cs6b	-5.4945	-38.6709	110	19/05/2003 - 15/06/2005	yes

itpb	-15.9887	-39.6282	307	12/10/2002 - 03/05/2004	yes
pdcb	-12.5306	-39.1238	220	24/09/2002 - 25/02/2004	yes
trsb	-4.873	-42.7059	125	12/10/2002 - 03/05/2004	yes
Bodes (Broadband Stations					
ar01	-6.1682	-39.4098	305	11/02/2015 - 22/02/2016	yes
ar02	-6.6419	-39.3402	341	02/02/2015 - 18/02/2017	yes
ar03	-7.0466	-39.4958	479	02/02/2015 - 07/06/2016	no
ar04	-7.5758	-39.6746	493	07/01/2015 - 18/02/2017	yes
ar05	-8.0932	-39.8983	441	02/02/2015 - 18/02/2017	yes
ar06	-8.6305	-40.2249	454	02/02/2015 - 24/08/2016	yes
ar07	-9.6154	-40.3837	405	02/02/2015 - 25/12/2016	yes
ar08	-9.1450	-40.3727	394	13/02/2015 - 21/08/2016	no
ar09	-10.2136	-40.1954	678	07/06/2016 - 24/04/2017	yes
ar50	-7.2079	-39.5494	920	19/09/2015 - 21/06/2016	no
ar51	-7.3879	-39.6314	933	11/06/2015 - 11/06/2015	no
Others (Broadband Stations)					
jcbe	-5.446	-35.775	114	28/10/2011 - 14/11/2012	no
pcsc	-8.35	-36.191	582	27/08/2012 - 14/12/2012	no

Figure S1 displays harmonic stripping results for each station. The five coefficient functions (A(z), B(z), C(z), D(z) and E(z)) - obtained by solving equation 1 - are represented in the upper part of the figure. The lower part represents the energy functions for the k=1 and k=2 harmonic degrees (see section 3). Note that, for most stations, energy on the k=1 and k=2 harmonic degrees are of comparable strength.

Figure S2 displays the k=1 and k=2 energy functions (see section 3) obtained for a synthetic receiver function test. We present 4 velocity models consisting of 3 layers with constant Vp and Vs. Layer 2 (in the middle) is characterized by anisotropy with an horizontal (first case - 0°) or dipping (following cases - 10°, 15°, 20°) fast axis of symmetry. Note that, for a horizontal axis of symmetry, the energy is entirely on the k=2 harmonic and that, when increasing the dip of the axis of symmetry, more energy becomes visible on the k=1 degree. For a slightly dipping axis of symmetry (10-to-15°), energy on both k=1 and k=2 degrees are of similar strength. And for a 20° dip, energy is dominant on the k=1 harmonic.

Figure S3 is an example of recorded radial and transverse receiver functions at station CS6B. Receiver functions are plotted as a function of back-azimuth. The transverse component record amplitude for mantle depths but no periodic pattern is visible. This "non-azimuthal" anisotropy has similar energy than azimuthal anisotropy recorded at other stations (see Figure 6).

AR01

harmonics

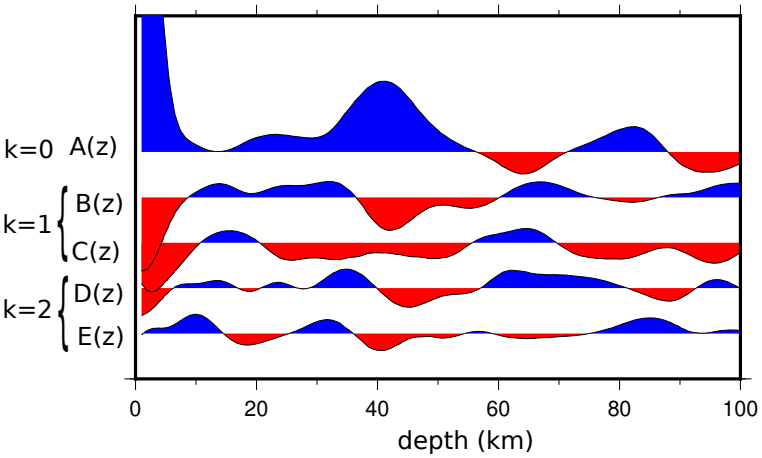

energy

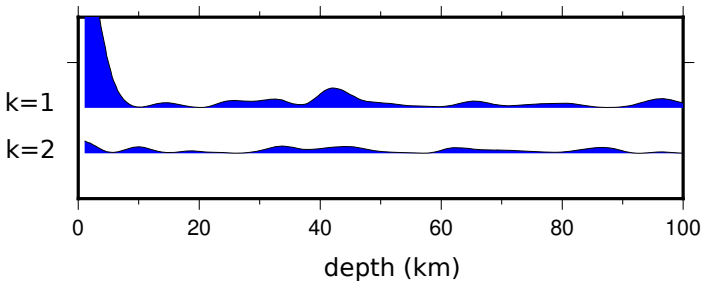

AR02

harmonics

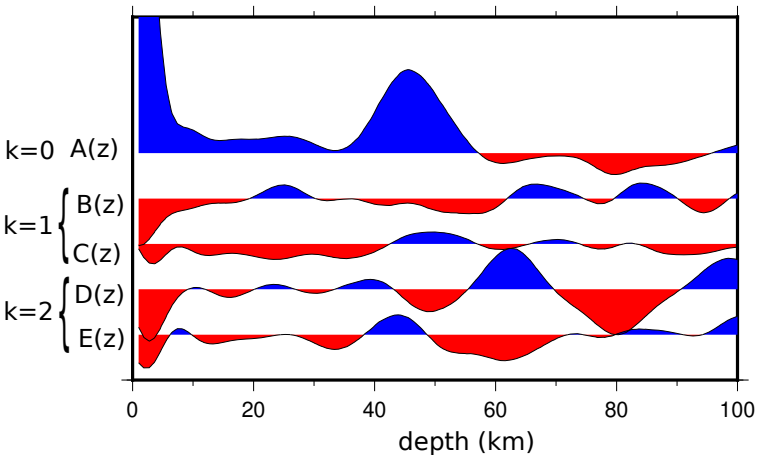

energy

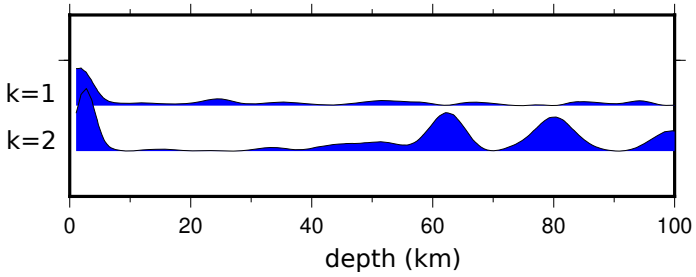

AR04

harmonics

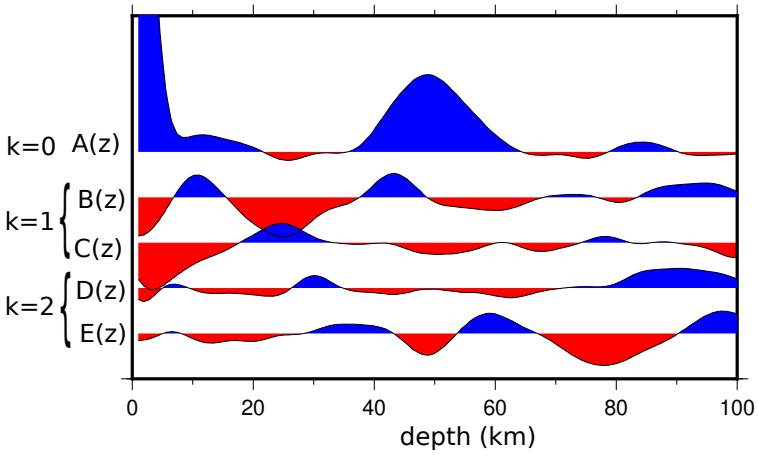

energy

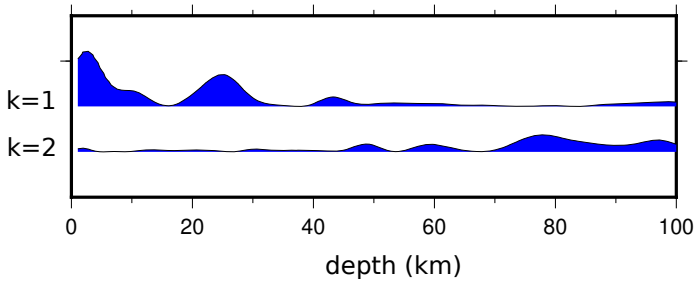

AR05

harmonics

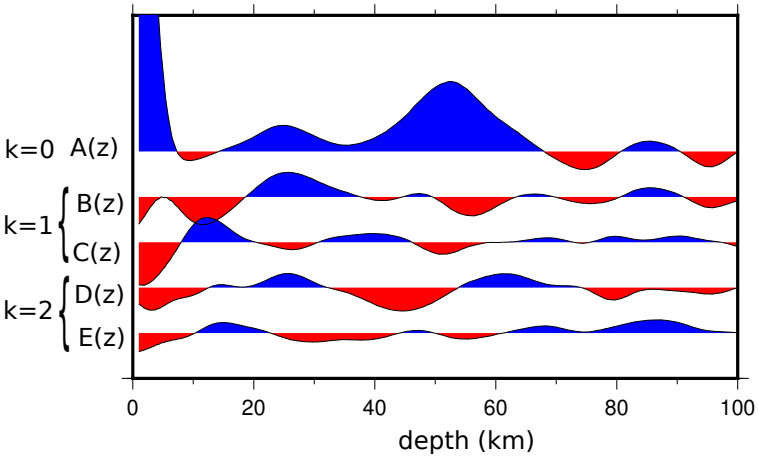

energy

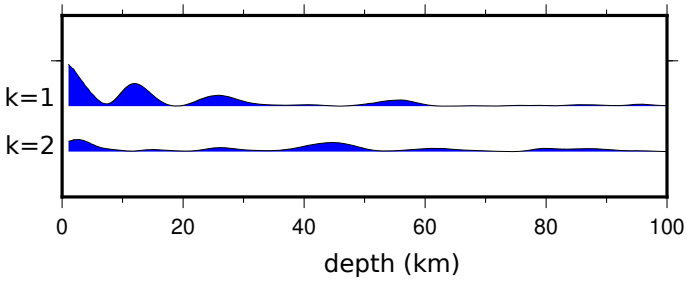

AR06

harmonics

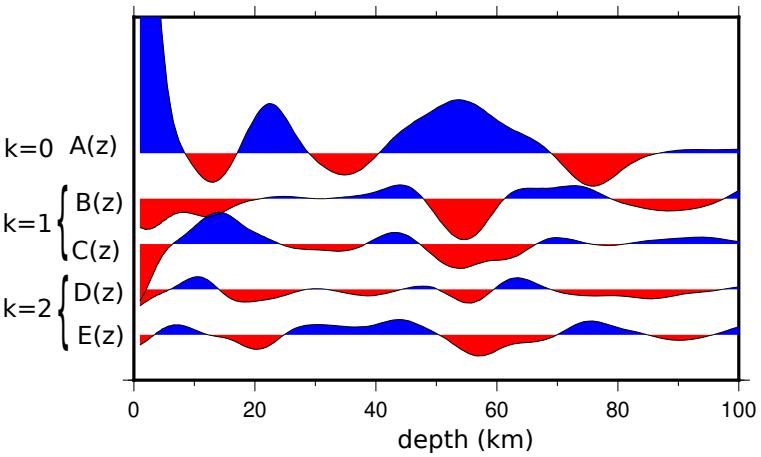

energy

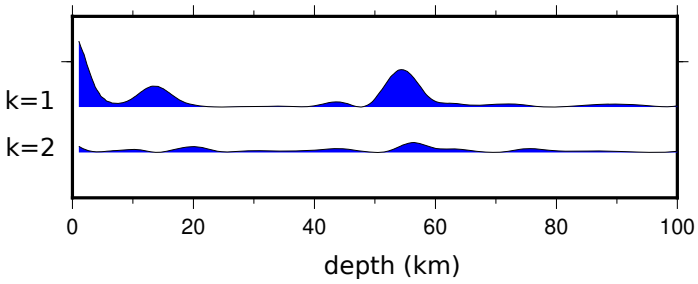

AR07

harmonics

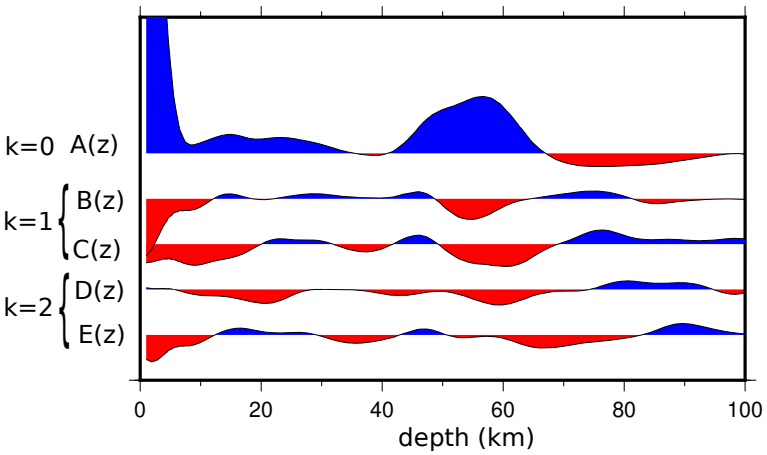

energy

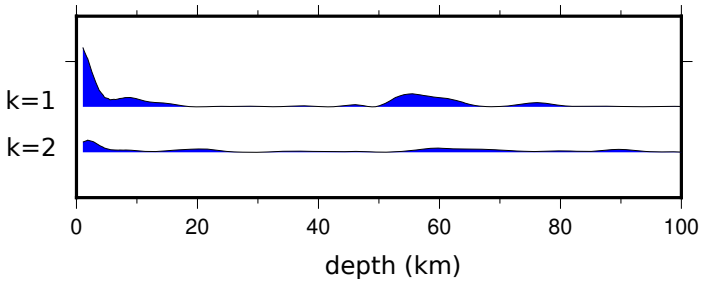

AR09

harmonics

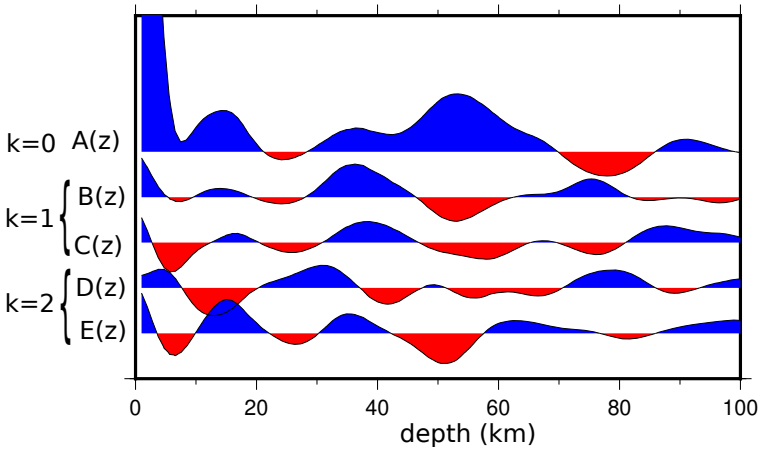

energy

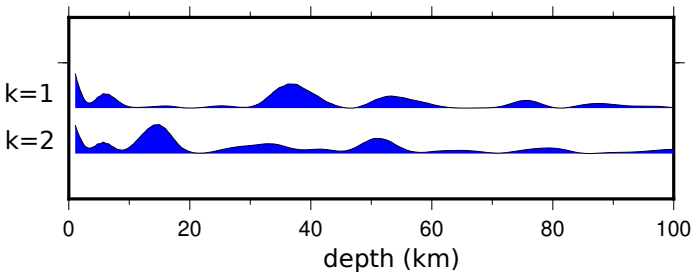

CAUB

harmonics

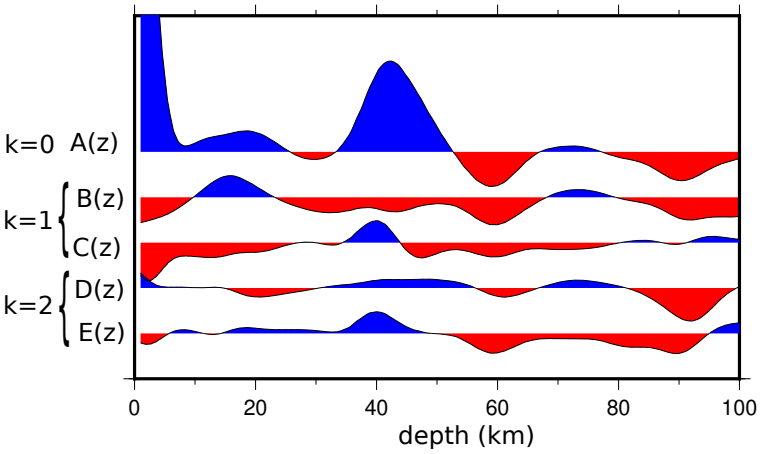

energy

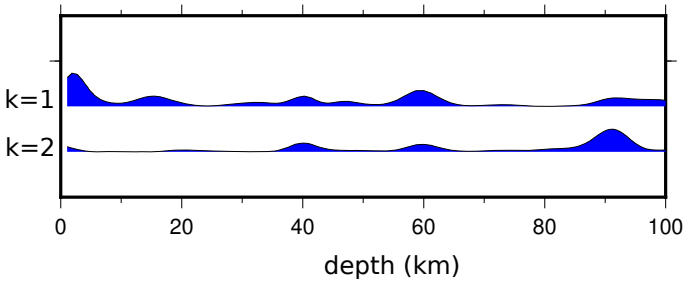

CS6B

harmonics

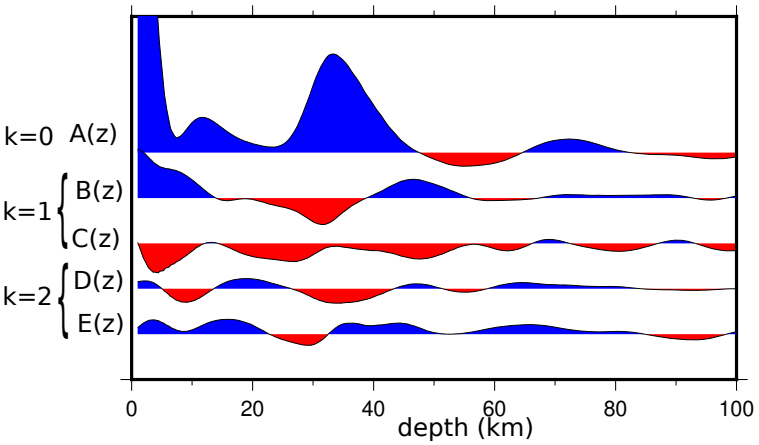

energy

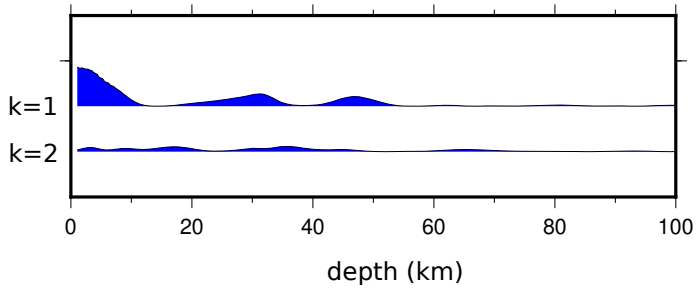

ITPB

harmonics

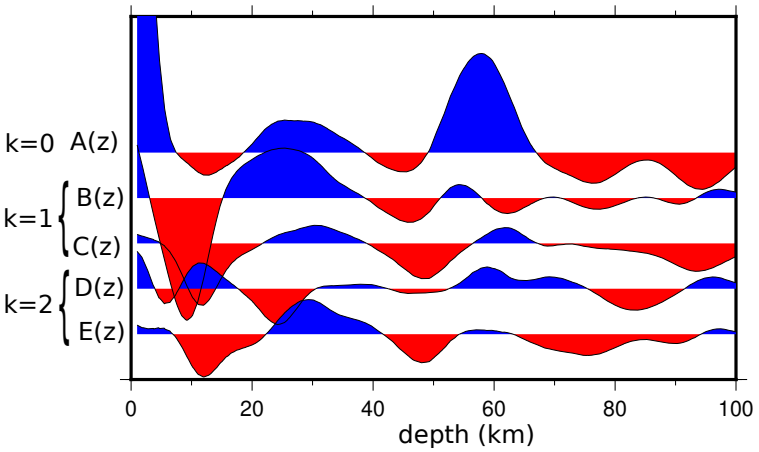

energy

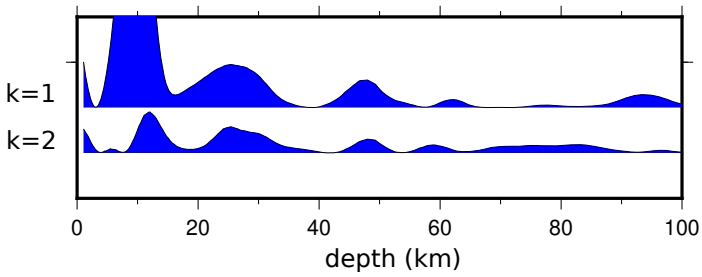

KM60

harmonics

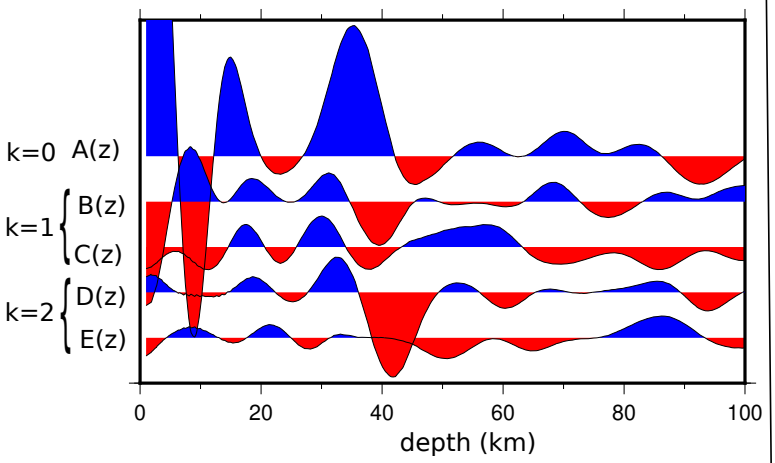

energy

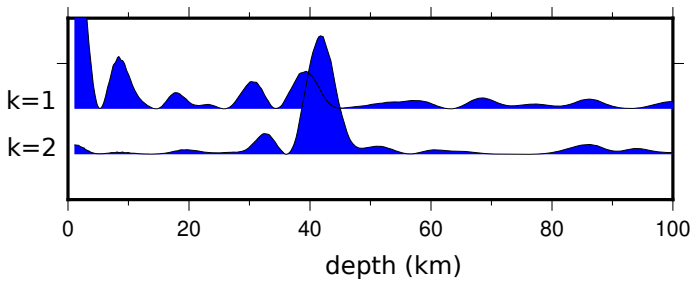

LP02

harmonics

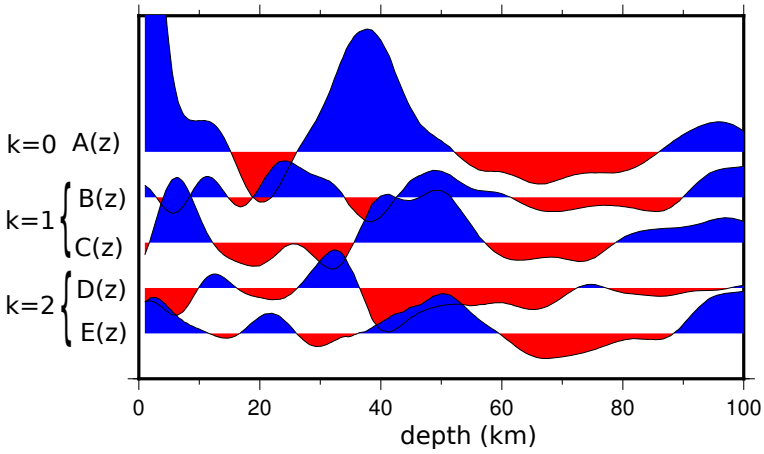

energy

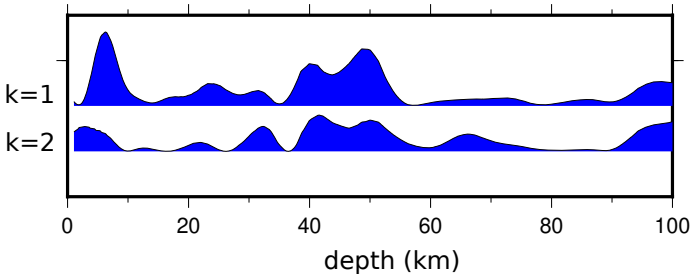

LP06

harmonics

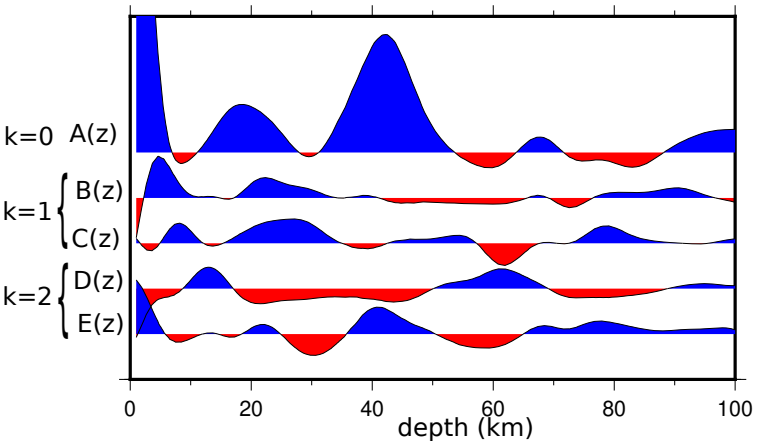

energy

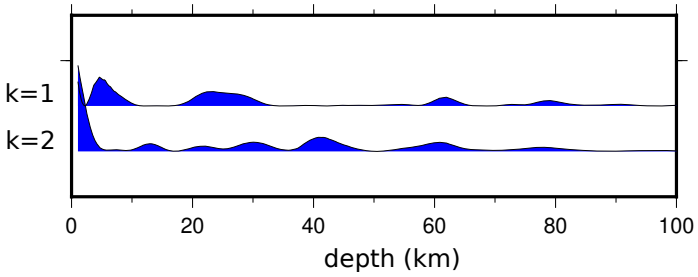

NBAN

harmonics

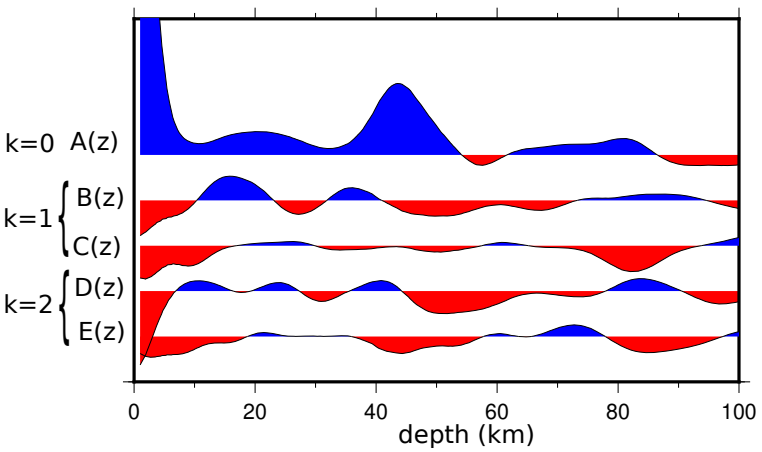

energy

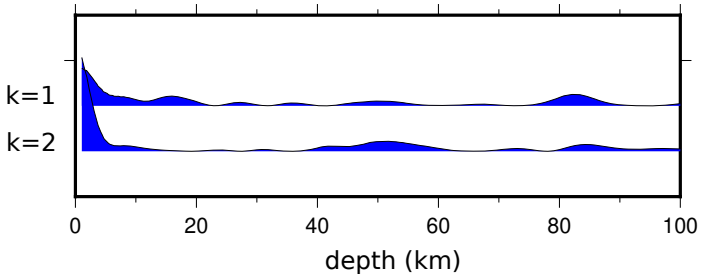

NBCL

harmonics

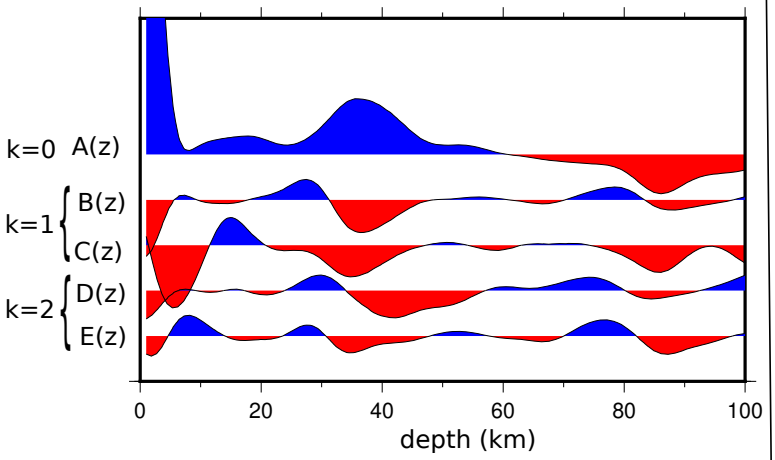

energy

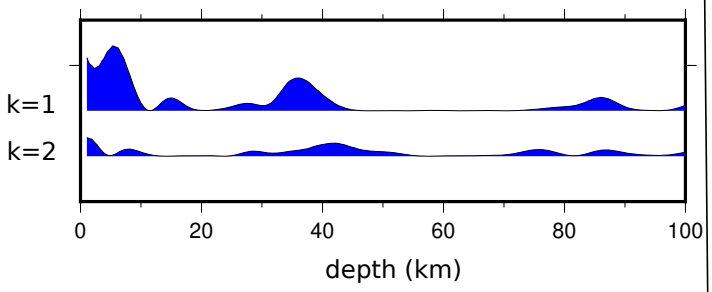

NBCP

harmonics

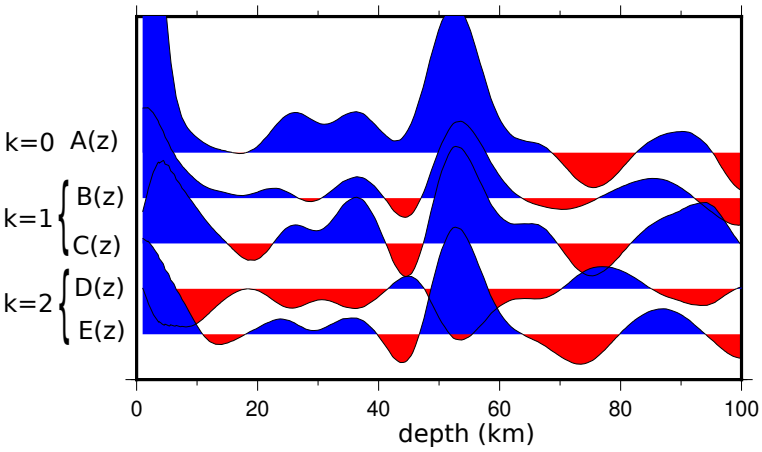

energy

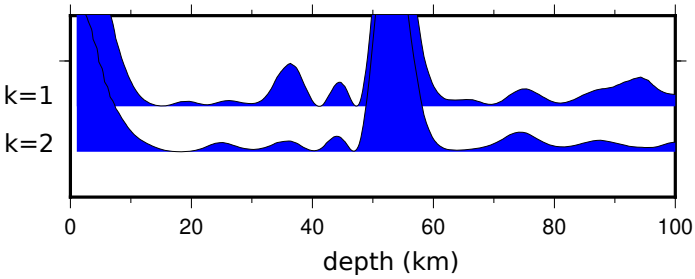

NBIT

harmonics

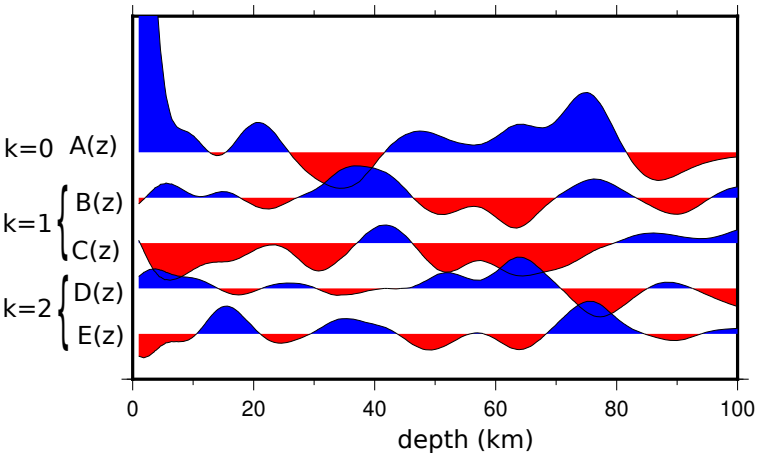

energy

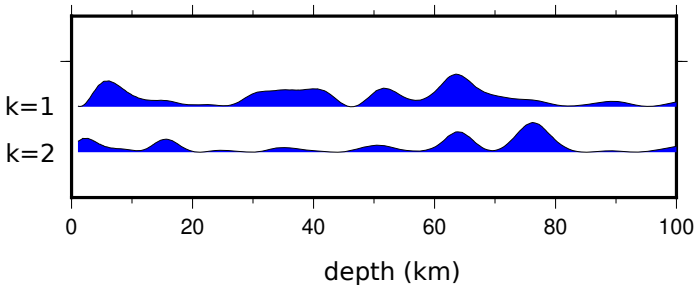

NBLA

harmonics

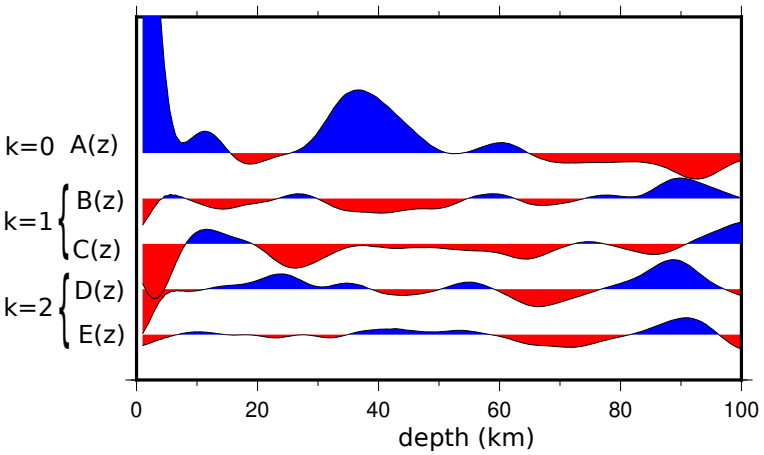

energy

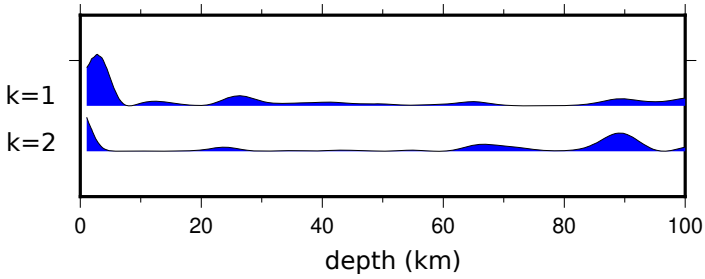

NBLI

harmonics

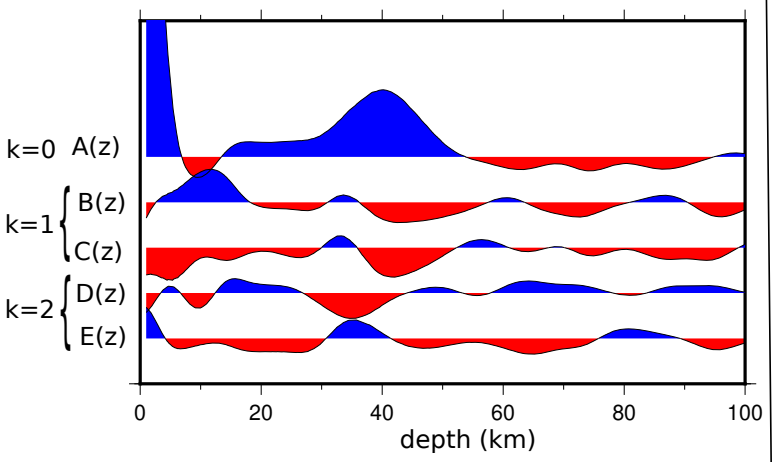

energy

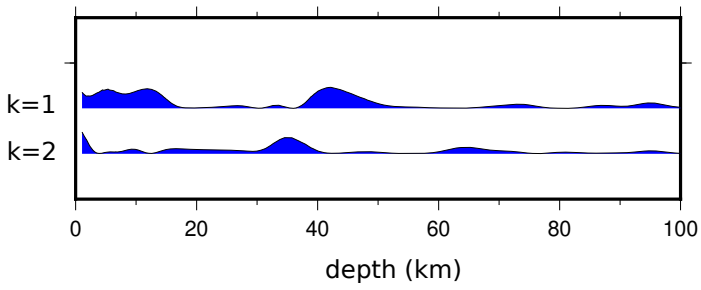

NBMA

harmonics

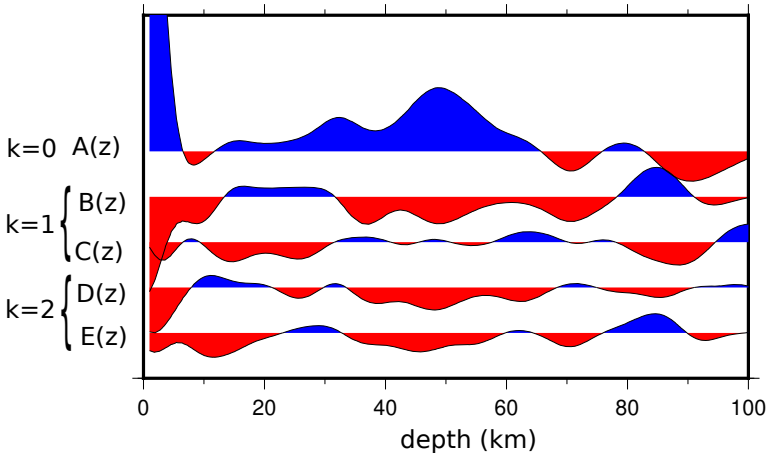

energy

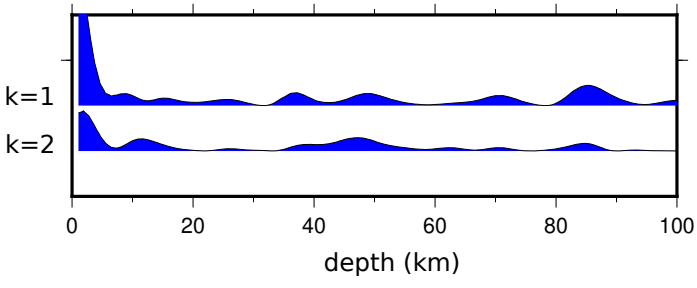

NBMO

harmonics

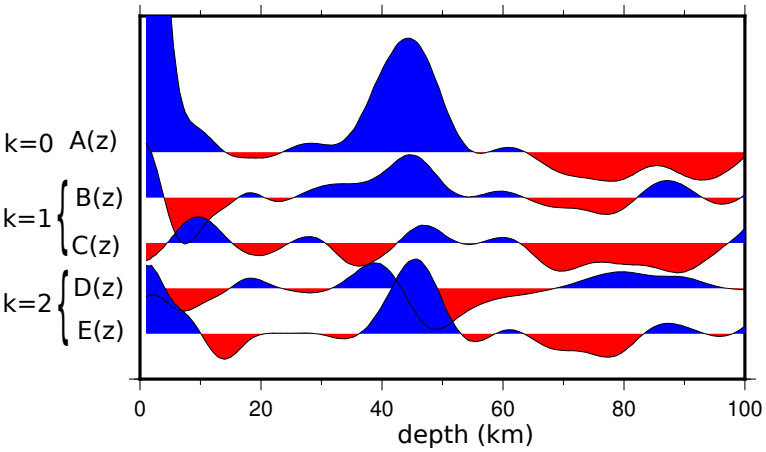

energy

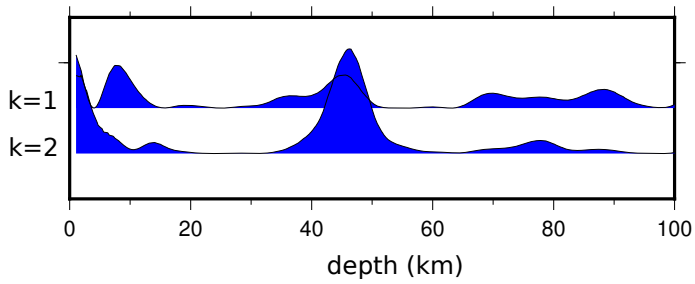

NBPA

harmonics

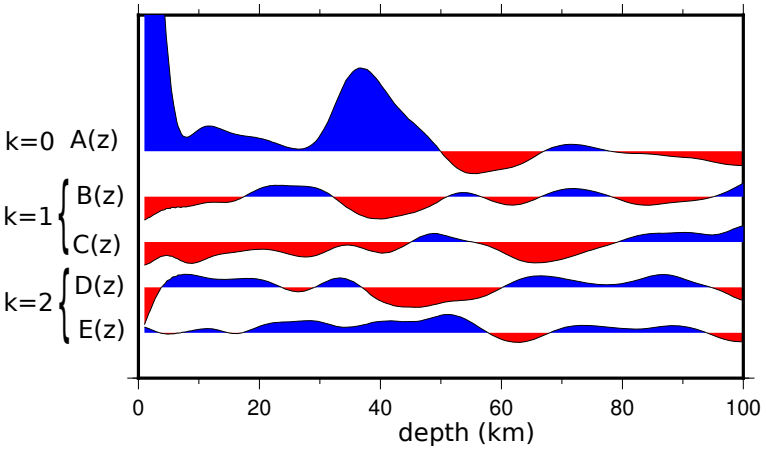

energy

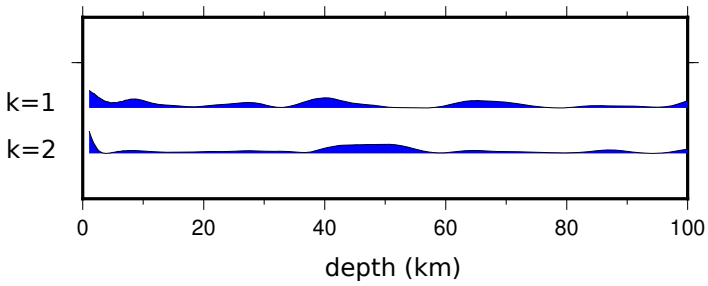

NBPB

harmonics

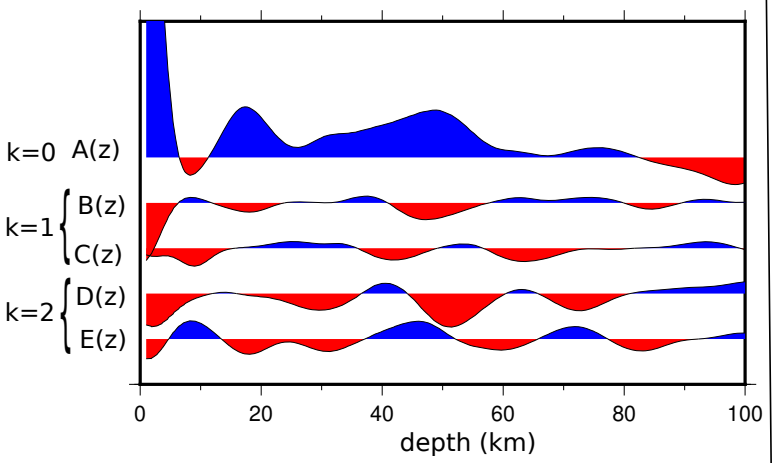

energy

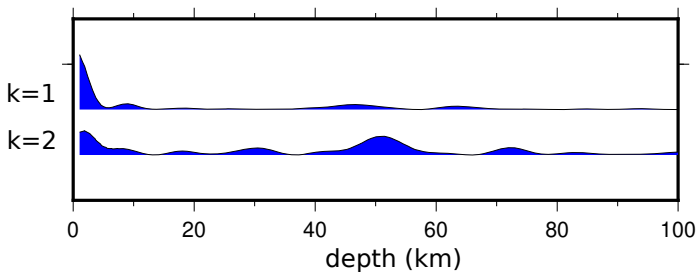

NBPN

harmonics

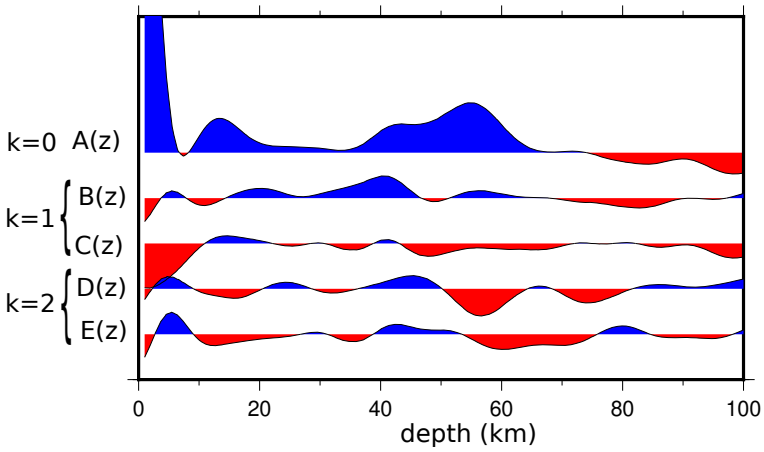

energy

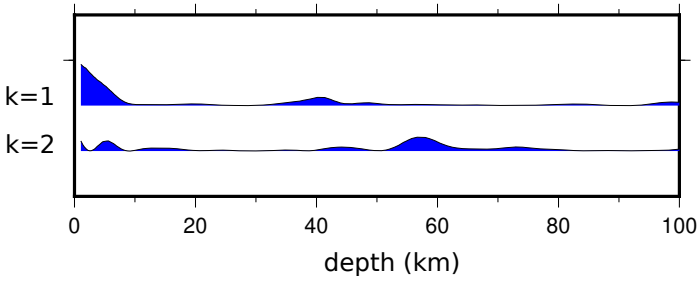

NBPS

harmonics

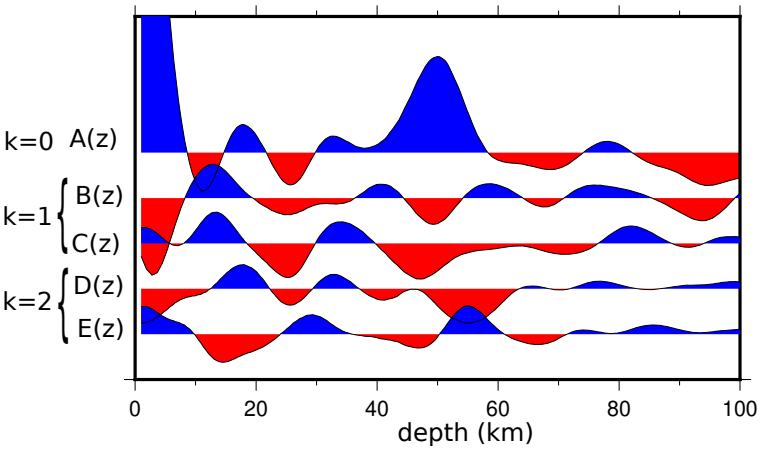

energy

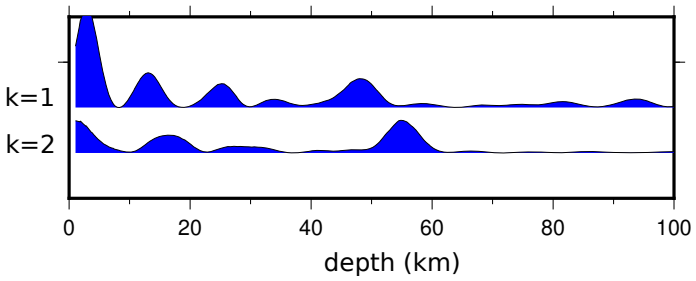

NBPV

harmonics

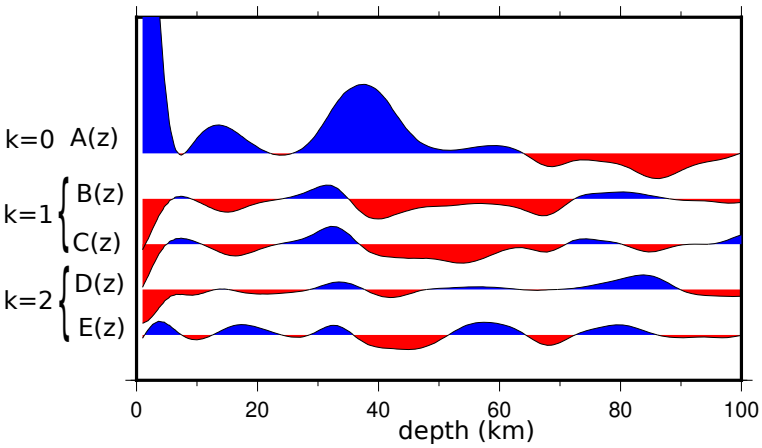

energy

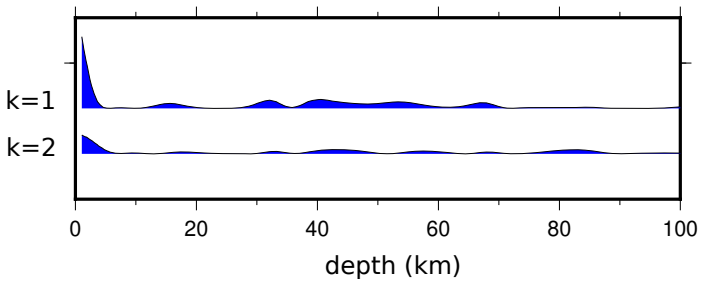

NBRF

harmonics

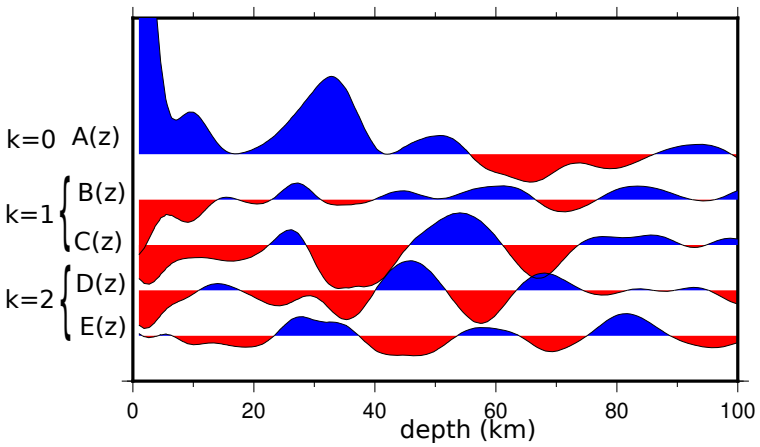

energy

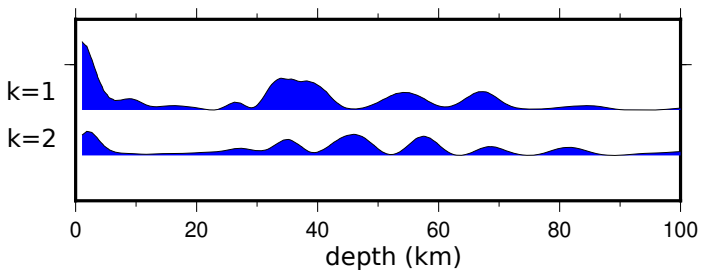

NBTA

harmonics

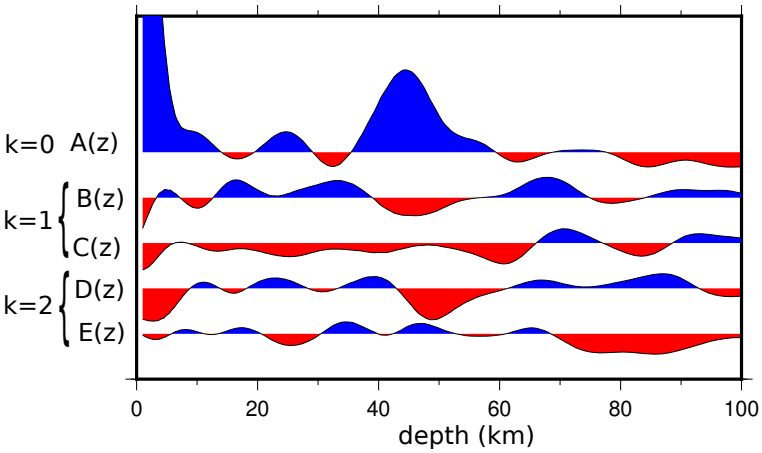

energy

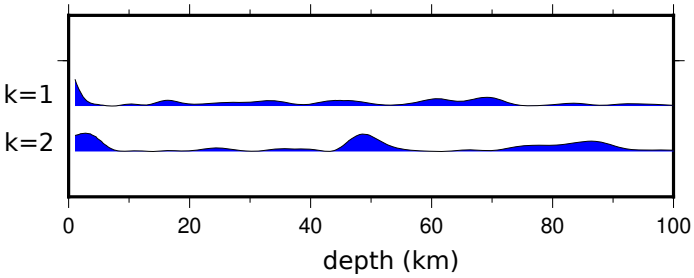

OCBR

harmonics

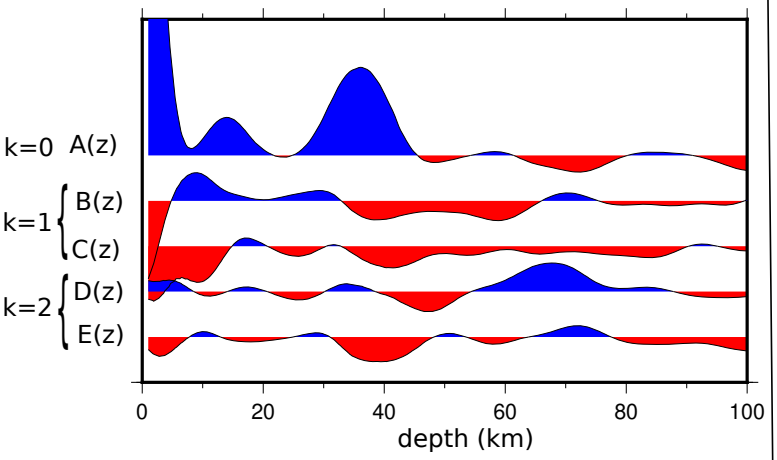

energy

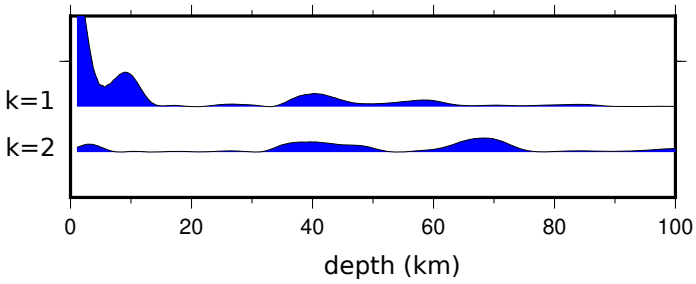

PCAL

harmonics

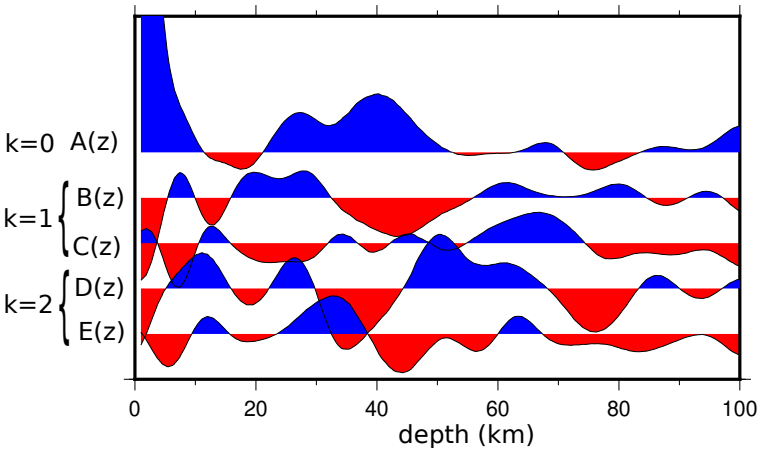

energy

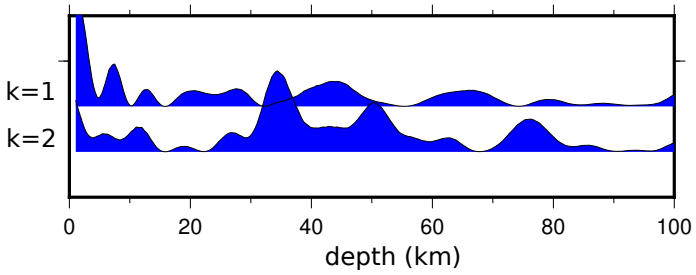

PCJA

harmonics

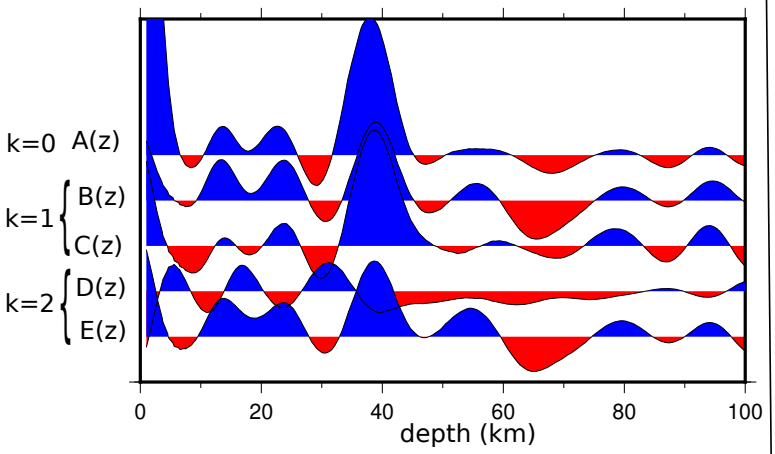

energy

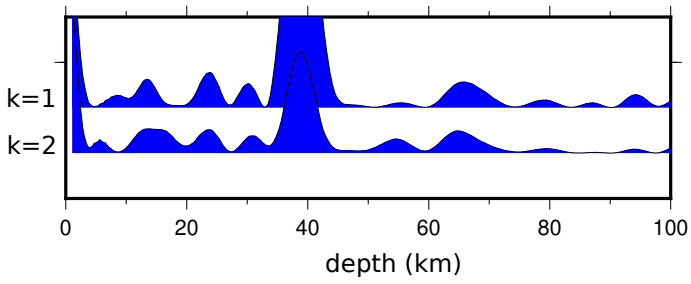

PCSA

harmonics

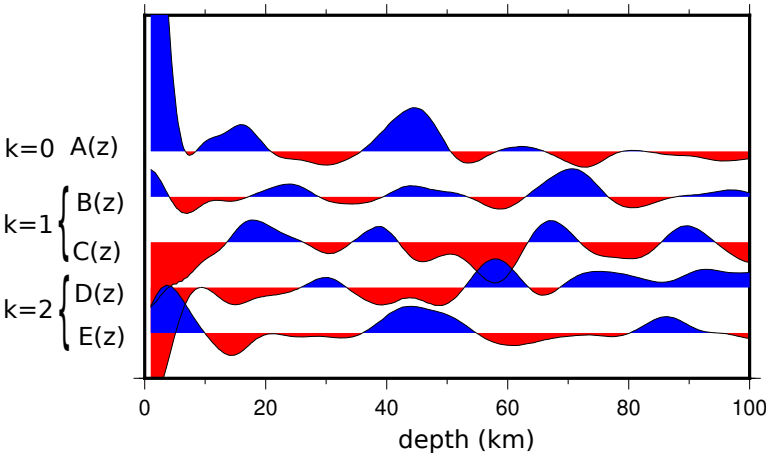

energy

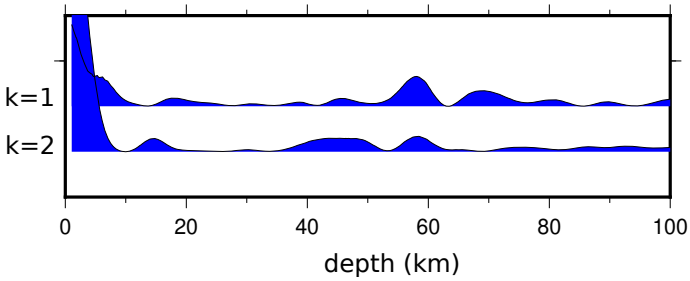

PCSE

harmonics

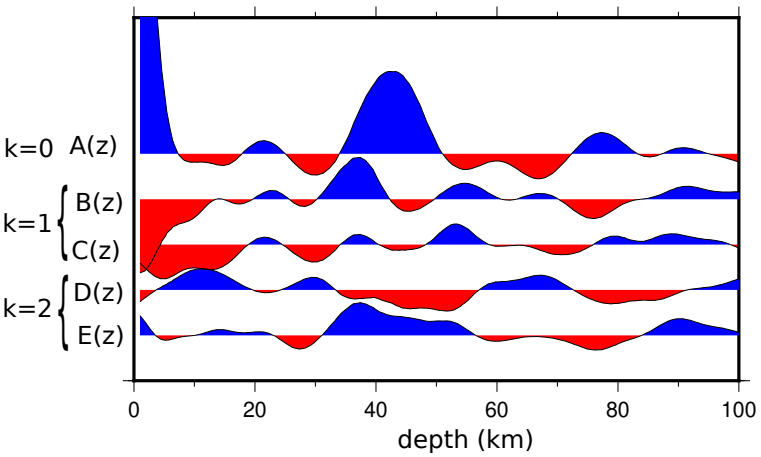

energy

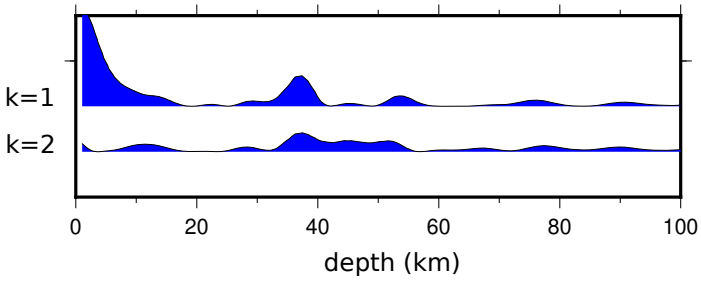

PCSL

harmonics

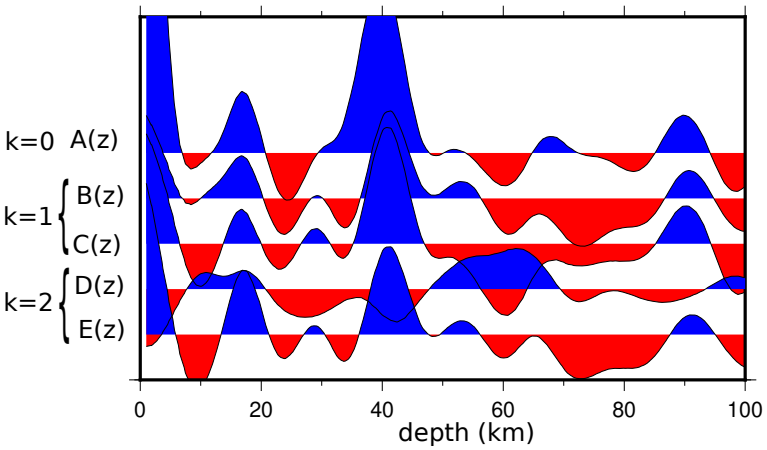

energy

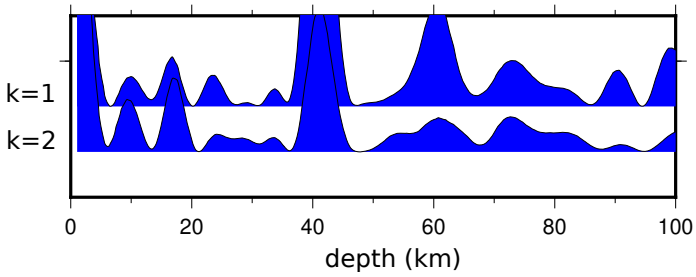

PCTV

harmonics

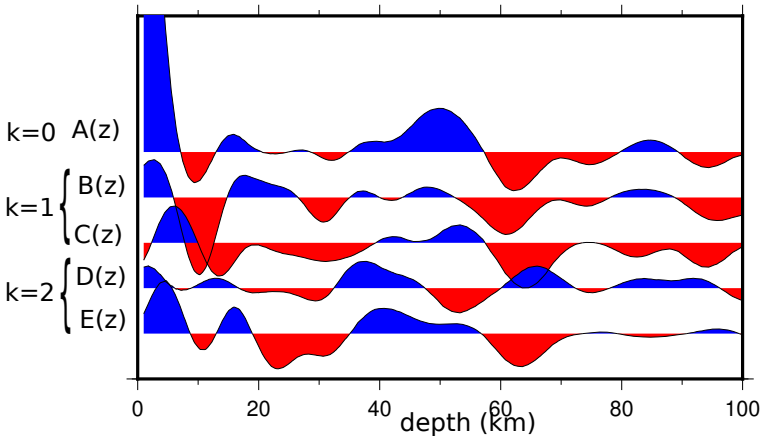

energy

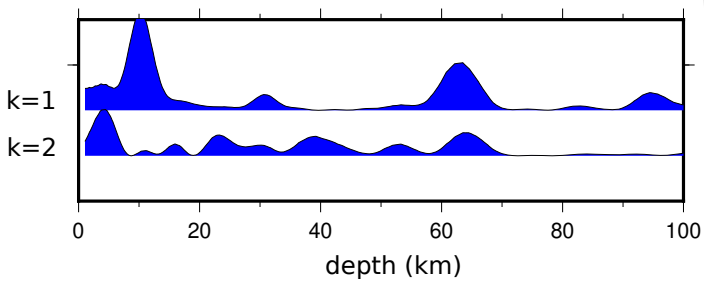

PDCB

harmonics

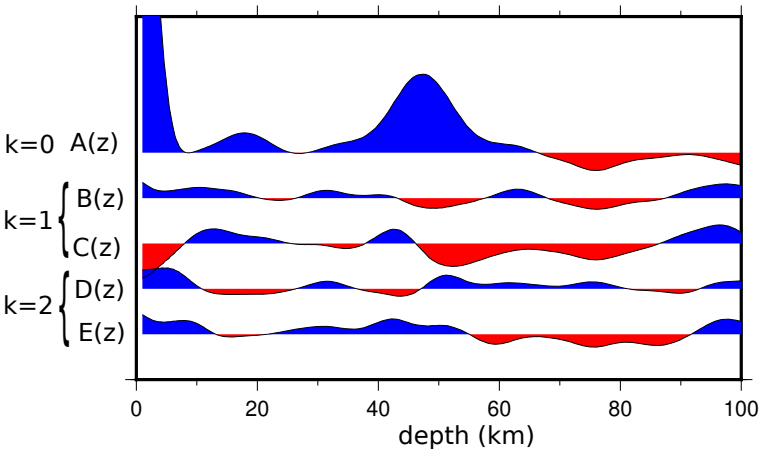

energy

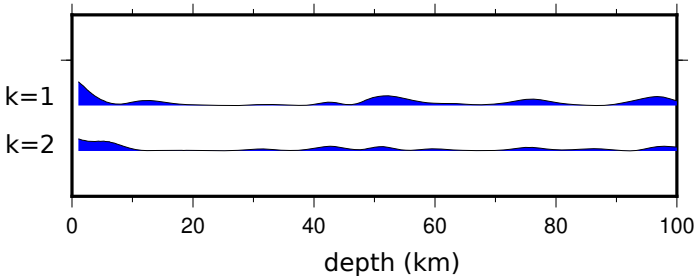

PFBR

harmonics

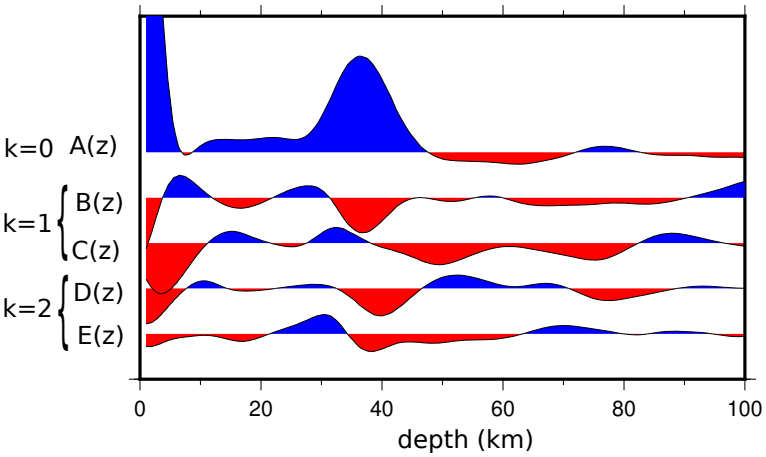

energy

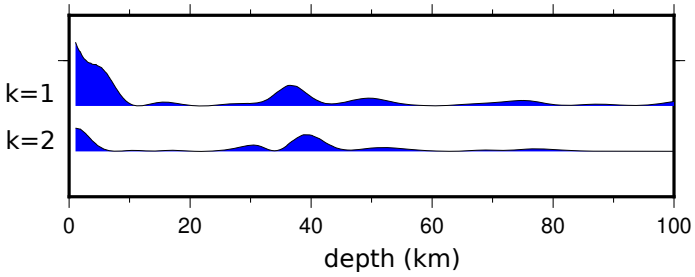

RCBR

harmonics

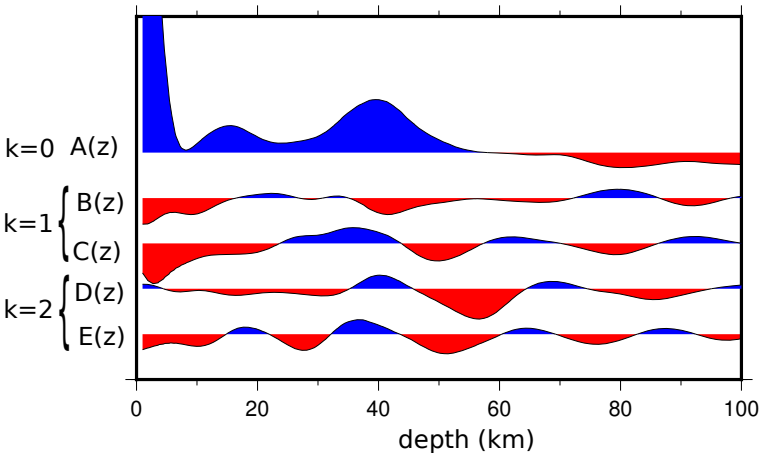

energy

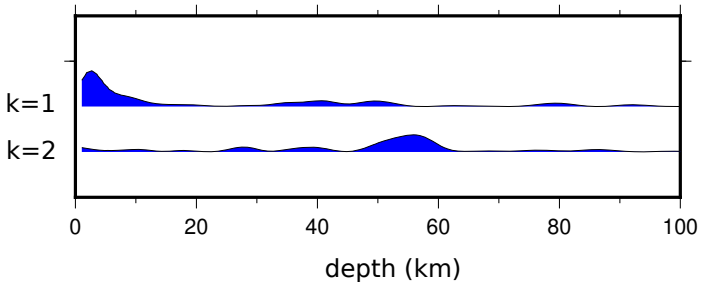

SABR

harmonics

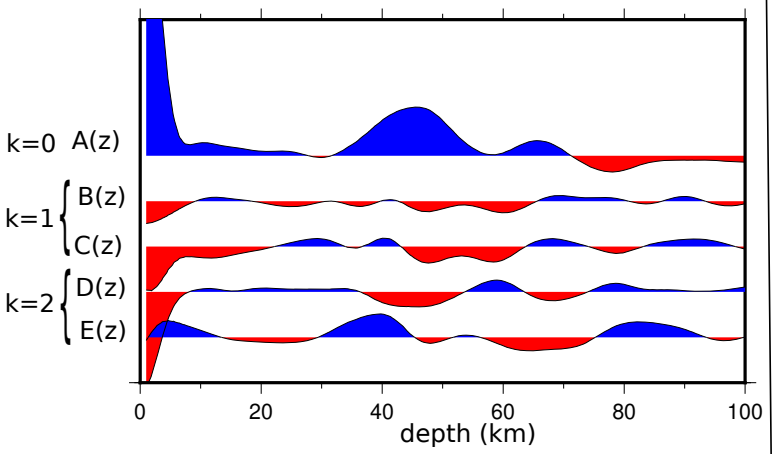

energy

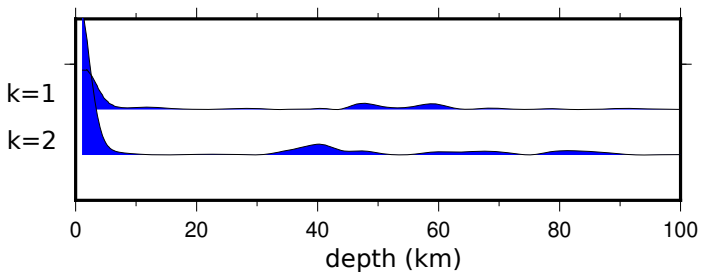

SBBR

harmonics

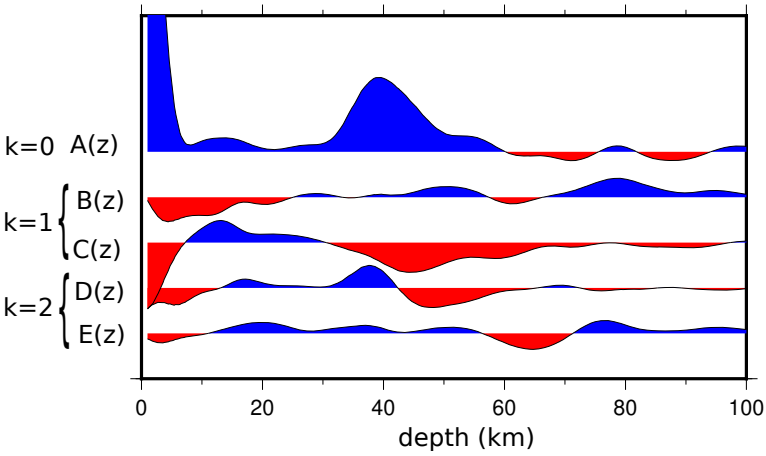

energy

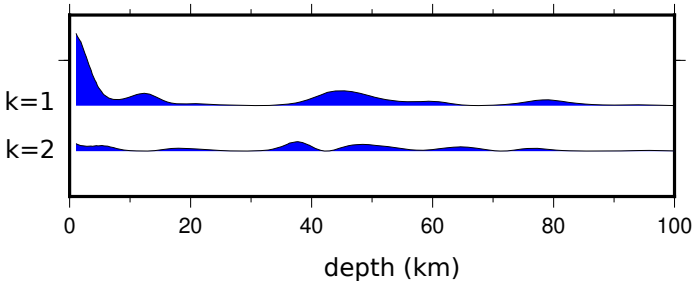

TRSB

harmonics

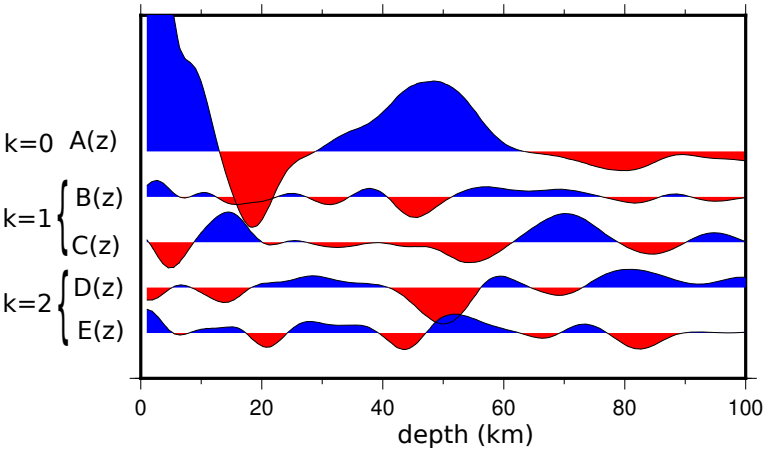

energy

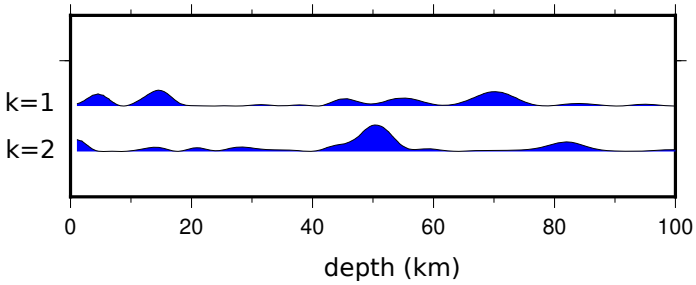

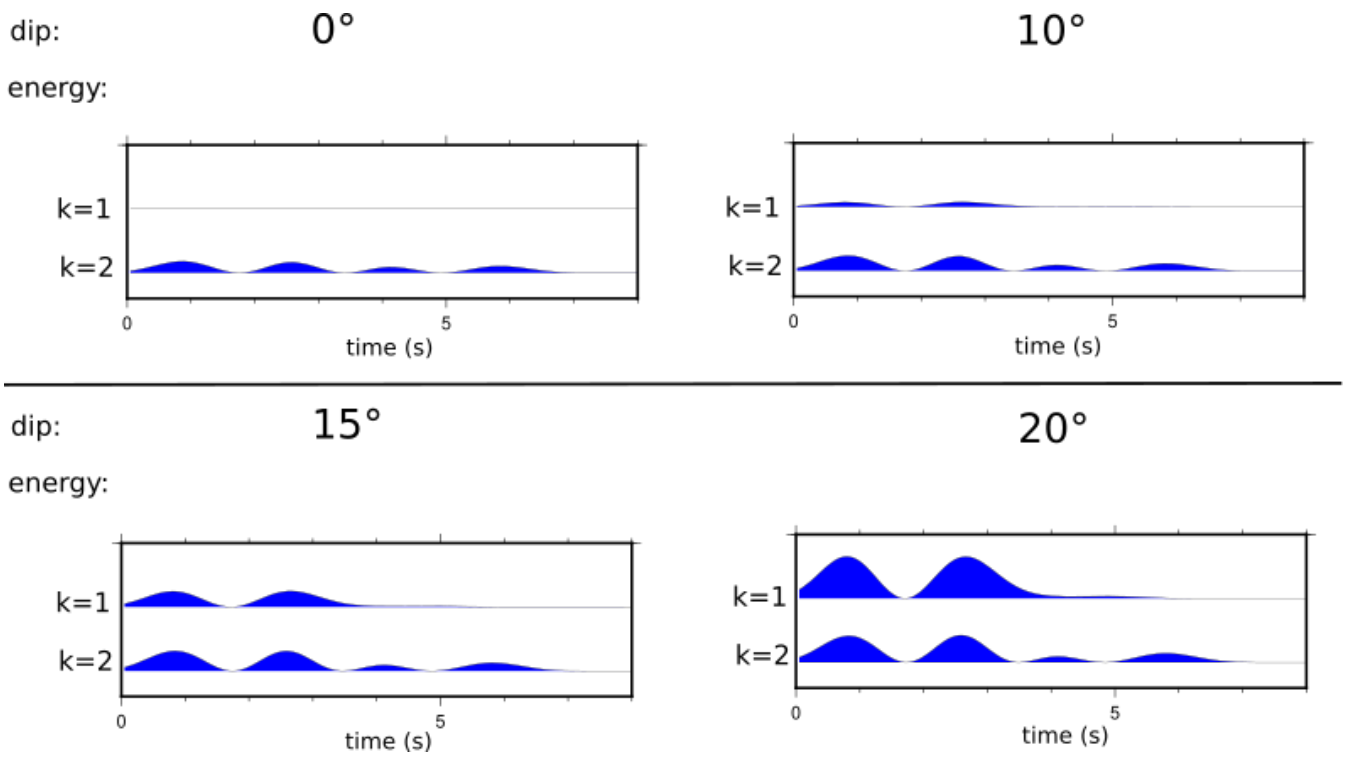

Figure S2. Energy on k=1 and k=2 harmonics are calculated for synthetics within a velocity model with 3 layers and constant Vp and Vs. The first and third layers are isotropic whereas the second layer display 6% anisotropy for both P and S-waves with fast axis dipping indicated above each corresponding graph (0, 10, 15 and 20°).

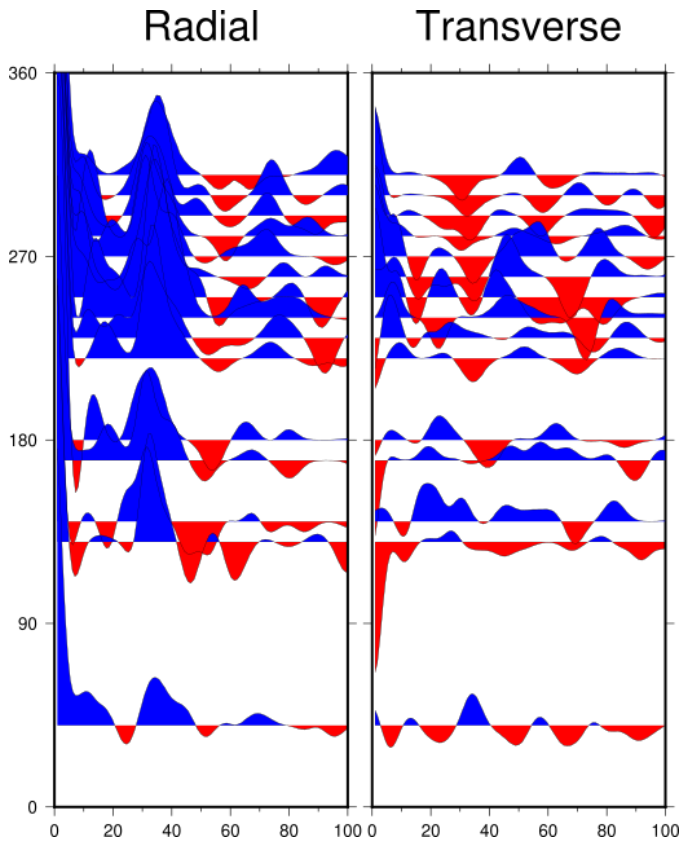

Figure S3. Radial and transverse receiver functions at station CS6B